

UTRECHT UNIVERSITY

INSTITUTE FOR MARINE AND ATMOSPHERIC  
RESEARCH UTRECHT

BACHELORTHESIS

---

# Fluid Dynamics near and at the Equator

---

*Author:*  
S.K.J. Falkena

*Supervisor:*  
Prof. Dr. L.R.M. Maas

June 17, 2014

## **Abstract**

The dynamics of a water basin at the equator is described using the lowest moments of its density and momentum fields; the centre-of-mass and the angular momentum around it. In the resulting model a non-conventional Coriolis term is used to describe the dynamics at the equator. Neglecting viscosity and diffusion, in the absence of wind and differential heating, a fluid pendulum in the equatorial plane is found. Adding differential heating in the zonal direction causes a deviation from this path. When mixing of momentum happens fast compared to mixing of temperature and salt stable points in and outside the equatorial plane are found taking one forcing at a time into account. Focussing on El Niño numerical computations show a downward jump of the centre-of-mass when the trade winds weaken. Seasonal variations at the Pacific Ocean cause periodic solutions to occur when forcings are strong. When evaporation is dominant chaos can be found.

# Contents

<b>1</b>	<b>Introduction</b>	<b>2</b>
<b>2</b>	<b>Dynamics of the centre-of-mass on the equator</b>	<b>4</b>
<b>3</b>	<b>Ignoring diffusion, viscosity and forcing</b>	<b>6</b>
3.1	A well-mixed state . . . . .	8
3.2	Oscillations in the equatorial plane . . . . .	9
<b>4</b>	<b>Ignoring diffusion and viscosity</b>	<b>11</b>
4.1	Forced oscillations in the equatorial plane . . . . .	12
4.1.1	Vertical differential buoyancy fluxes . . . . .	13
4.1.2	Zonal differential buoyancy fluxes . . . . .	13
<b>5</b>	<b>Dominant mixing of momentum</b>	<b>15</b>
5.1	Without forcing . . . . .	18
5.2	Equatorial symmetric forcings . . . . .	19
5.2.1	Zonal winds . . . . .	20
5.2.2	Zonal differential buoyancy fluxes . . . . .	21
5.2.3	Vertical differential buoyancy fluxes . . . . .	24
<b>6</b>	<b>El Niño</b>	<b>27</b>
6.1	Forcings during El Niño . . . . .	27
6.2	Dynamics of El Niño . . . . .	28
6.3	Seasonal variations . . . . .	29
<b>7</b>	<b>Discussion and conclusion</b>	<b>32</b>
<b>A</b>	<b>Reducing to three equations</b>	<b>35</b>

# 1 Introduction

The climate on earth affects us all. We check the weather forecasts to see whether we can go to the beach. We want to know which airstrip a plane has to use to land safely. We wonder what the effects are of continued emission of carbon dioxide on the temperature and what the consequences for the sea level are. For these and many more reasons research of the climate is important and interesting.

For 2014-2015 an extreme El Niño is predicted [1]. The consequences may be immense, particularly in the regions around the Pacific Ocean. El Niño's disrupt the normal weather patterns, causing for example floods in usually dry regions in South-America. El Niño is still not fully understood and research will remain necessary in the coming years.

El Niño is a quasi-periodic phenomenon occurring in the equatorial region of the Pacific Ocean [2]. During a couple of months the sea surface temperature at the east side of the Pacific Ocean around the equator is much higher than usual (by 6-8°C). The counterpart of El Niño is known as La Niña. During La Niña the sea surface temperature near South America is lower than usual (by 3-5°C). The El Niño-La Niña cycle has a quasi-period of two to seven years.

Usually the wind above the equator blows towards the west (trade winds), taking the warm surface water with it. This causes upwelling of cold water at the east side of the Pacific Ocean, which makes sea life flourish as the upwelling water is rich in nutrients. As a consequence the sea surface temperature in the west is several degrees higher than in the east, as can be seen in Figure 1. Also the thermocline, indicating at which depth the temperature decreases fastest with depth, is shown in this figure. In the atmosphere a convective circulation takes place (Figure 1). Air rises at the west side and descends at the east side.

During an El Niño the trade winds are weaker and the surface water at the east side of the ocean is warmer than in the normal situation (Figure 1). This is a self-sustaining situation; the smaller temperature difference between the east and west side weakens the wind, while the weaker wind takes less water towards the west and thus lowers the temperature difference. During an El Niño the thermocline lowers at the east side of the basin. Also the circulation in the atmosphere is disrupted. The region where most of the air rises moves towards the centre of the Pacific Ocean, causing eastward winds at the west side of the Pacific Ocean.

During a La Niña the opposite happens. The trade winds increase in strength and the sea surface temperature at the east side is lower than usual. The thermocline is closer to the surface near South-America indicating stronger upwelling. The region where air rises is located even further towards the west. A La Niña often follows an El Niño, causing mostly opposite weather to El Niño. For example during an El Niño there is a lot of rain at the coast of Peru, whilst during a La Niña it is very dry.

As El Niño takes place near the equator, it is very interesting to consider the dynamics of the equatorial region. On a rotating sphere, like the earth, this rotation affects the way fluids behave. The effects are described by the Coriolis force [3], which is proportional to the cross product of the earth's rotation vector ( $\Omega \propto (0, \cos \phi, \sin \phi)$ , with  $\phi$  the latitude) and the velocity of a particle. Most climate models use an f-plane approximation to describe the Coriolis force, where  $f \propto \sin \phi$ . In this approximation the horizontal component of the earth's

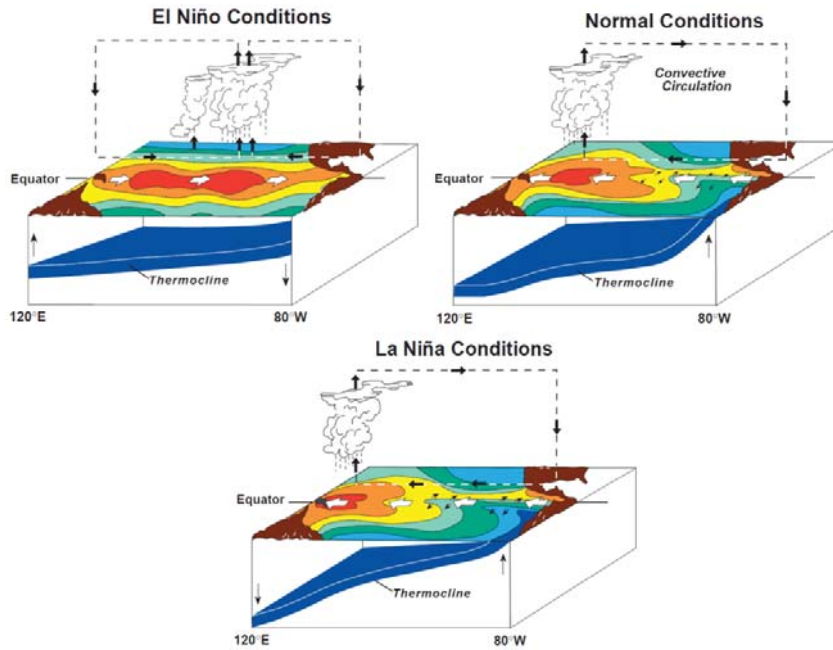


**Figure 1:** The sea surface temperature (red being above 30°C and dark blue below 20°C), wind, thermocline and areas of rising air during El Niño, La Niña and normal conditions. [1]

rotation vector is neglected. This however is not valid at the equator since then  $f = 0$ . Therefore it is important and interesting to abandon this approximation and look specifically at the situation at the equator employing non-traditional Coriolis terms.

In this thesis a model that describes the dynamics of the ocean in terms of the lowest moments of the density and momentum fields is used. This means we look at the location of the centre-of-mass and the angular momentum around it in a box of water on the equator. It is important to note we will look at an ocean-only model instead of a coupled ocean-atmosphere model as is customary. Even in this low order ocean-only model the non-linear terms are able to produce ‘rich’ dynamics. Looking at low order dynamics allows us to describe the ocean using ordinary differential equations, while for higher order terms partial differential equations are needed. It also provides us with more insight in the dynamics, as we can follow the movement of the centre-of-mass in detail. This way it is possible to better understand the causes and consequences of the dynamics.

We will focus on the consequences of the non-traditional Coriolis term in our low order model. To acquire better insight at the dynamics at the equator, we will approximate our model in various ways. These approximations will be mostly focussed on obtaining solutions in an analytical manner. Numerical methods are used when analytical solutions can not be easily acquired any more.

## 2 Dynamics of the centre-of-mass on the equator

Maas (2004) [4] gives us the equations for the dynamics of the centre-of-mass at mid-latitudes in a certain basin. These first order ordinary (not partial!) differential equations for the location of the centre-of-mass  $\mathbf{X}$  and the basin-averaged angular momentum  $\mathbf{L}$  around it, describe the dynamics of the basin at lowest order. The equations are obtained by integrating the Navier-Stokes equations over the whole basin.

The location of the centre-of-mass  $\mathbf{X}(t)$ , with components  $X(t)$ ,  $Y(t)$  and  $Z(t)$ , is given in Cartesian coordinates  $\mathbf{x} = (x, y, z)$  on a plane tangent to the earth with its centre corresponding to the centre of the basin. We denote with  $\mathbf{i}$ ,  $\mathbf{j}$  and  $\mathbf{k}$  the unit vectors in the positive  $x$ ,  $y$  and  $z$  direction respectively. The  $x$ -direction is the zonal direction, with positive  $x$  pointing east. The  $y$ -direction is the meridional direction, with north corresponding to positive  $y$ . The  $z$ -direction is the vertical direction, with positive  $z$  pointing against gravity. In this coordinate system the basin-averaged angular momentum around the origin  $\mathbf{L}(t)$  has components  $L_1(t)$ ,  $L_2(t)$  and  $L_3(t)$ , which represents rotation around the  $x$ -,  $y$ - and  $z$ -axis respectively following the right-hand rule.

In this coordinate system the first order differential equations describing the behaviour of  $\mathbf{X}(t)$  and  $\mathbf{L}(t)$  are:

$$Pr^{-1} \frac{d\mathbf{L}}{dt} + f' \mathbf{k} \times \mathbf{L} = -Y\mathbf{i} + X\mathbf{j} - (L_1, L_2, rL_3) + \hat{T}\mathbf{T} \quad (1)$$

$$\frac{d\mathbf{X}}{dt} + \mathbf{X} \times \mathbf{L} = -(X, Y, \mu Z) + Ra\mathbf{F} \quad (2)$$

In these equations  $\mathbf{T}$  drives the angular momentum and in this way represents differential momentum fluxes due to wind stress.  $\mathbf{F}$  represents forcing due to differential buoyancy fluxes and drives the centre-of-mass directly. Furthermore  $Pr$  is a Prandtl number defined as  $Pr = \frac{r_h L^2}{12K_h}$  and measures the ratio of viscous over diffusive processes,  $\hat{T}$  gives the magnitude of the wind stress torque and  $Ra$  is a Rayleigh number defined as  $Ra = \frac{g\delta\rho_e H}{2r_h K_h \rho_0}$  and represents differential heating. In these definitions  $r_v$  and  $r_h$  represent Rayleigh damping coefficients in both vertical and horizontal directions (friction),  $L$  and  $H$  depict the length and depth of the basin,  $K_v$  and  $K_h$  represent diffusion in the vertical and horizontal direction,  $g$  is the gravitational acceleration,  $\delta\rho_e$  is the external density contrast (normalizing for the average density difference between east and west) and  $\rho_0$  is a constant reference density. Also  $r = \frac{r_v}{r_h}$  represents the friction-ratio and  $\mu = \frac{K_v L^2}{K_h H^2}$  the diffusion-ratio. Lastly  $f' = \frac{2\Omega \sin \phi}{2r_h}$ , with  $\Omega$  the rotation rate of the earth and  $\phi$  the latitude, represents the traditional Coriolis term due to the earth's rotation in an f-plane description.

In Maas (1994, 2004) [5] an f-plane approximation is made in which the  $y$ -part of the rotation vector  $\mathbf{\Omega}$ , proportional to  $\cos \phi$ , is neglected. This results in an approximation which is strictly speaking only valid on the poles, where  $\phi = \pm \frac{\pi}{2}$ . For higher latitudes this may be a reasonable approximation, but on the equator, where  $\phi = 0$ , it does not describe the Coriolis force correctly any more. To investigate the dynamics on the equator and especially El Niño we here abandon this approximation.

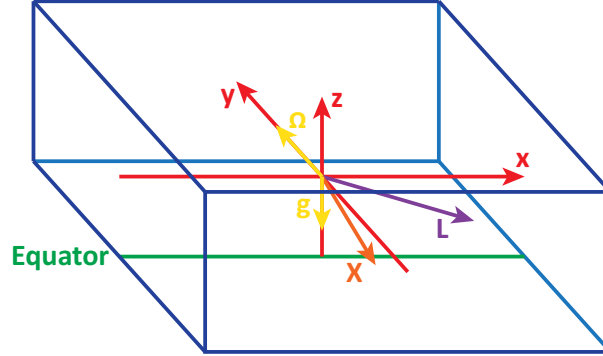


**Figure 2:** The box on the equator with the axes shown in red with arrows pointing in positive directions. Gravity  $g$  and the earth's rotation  $\Omega$  are depicted in yellow. The orange and purple arrows show possible vectors for  $\mathbf{X}$  and  $\mathbf{L}$  respectively.

To do so, the coordinate system has to be changed. We again use Cartesian coordinates, but now in a box tangent to the equator with its centre at the centre of the basin as depicted in Figure 2. The  $x$ -,  $y$ - and  $z$ -directions remain the same, hence  $x$  gives the longitude,  $y$  the latitude and  $z$  the altitude as can be seen in Figure 3. This time it is important to assume the basin has artificial walls at latitudes of  $\pm 2^\circ$ , since at higher latitudes the dynamics are observed to change drastically [6].

Now, to find the equations describing the dynamics at the equator, the only term we have to change with respect to (1) and (2) is the Coriolis term. On the equator the rotation of the earth has only a component in the  $y$ -direction, so the Coriolis acceleration takes the form of:

$$a_{coriolis} = 2\boldsymbol{\Omega} \times \mathbf{L} = 2\Omega \mathbf{j} \times \mathbf{L} \quad (3)$$

By changing the Coriolis term, the new equations describing the dynamics on the equator become:

$$Pr^{-1} \frac{d\mathbf{L}}{dt} + f\mathbf{j} \times \mathbf{L} = -Y\mathbf{i} + X\mathbf{j} - (L_1, L_2, rL_3) + \hat{T}\mathbf{T} \quad (4)$$

$$\frac{d\mathbf{X}}{dt} + \mathbf{X} \times \mathbf{L} = -(X, Y, \mu Z) + Ra\mathbf{F} \quad (5)$$

In this equations the unconventional horizontal component of the Coriolis acceleration reads  $f = \frac{2\Omega}{r_h + r_v}$ . Here we divide by  $r_h + r_v$  because the cross product gives rise to a Coriolis force in the zonal and vertical directions. Note that  $f$  is always positive, in contrast to the classical  $f'$  in (1) which can also be negative.

In the following sections we look at (4) and (5) in more detail and use various approximations to understand their behaviour. The approximations we make are mostly guided by simplifying the equations in a way we can solve them analytically. We will also look specifically at the forcings in the Pacific Ocean during the normal situation and El Niño and investigate the behaviour that follows from our model in these cases.

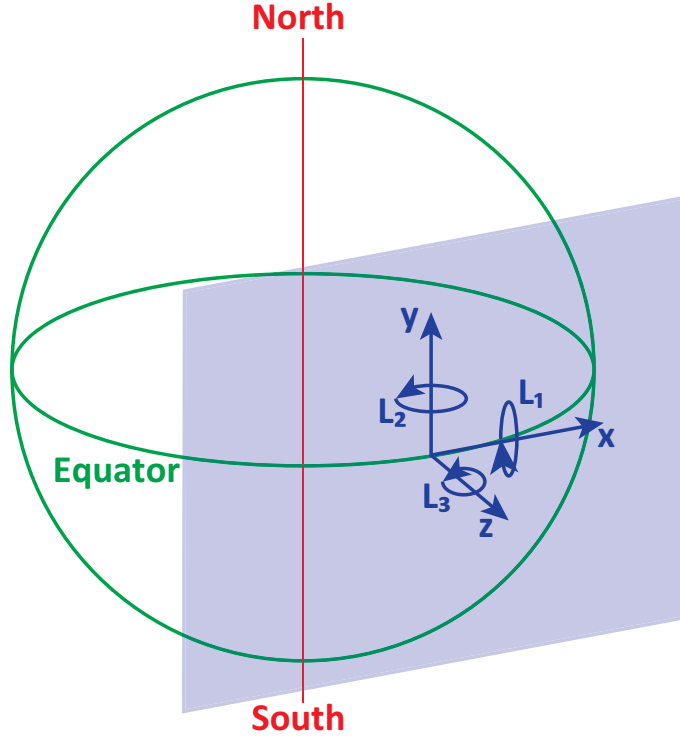


**Figure 3:** The coordinate system on earth with the arrows pointing in positive directions (rotation goes according to the right-hand rule).

### 3 Ignoring diffusion, viscosity and forcing

First we investigate one of the most simple cases, namely when there is no diffusion, viscosity or forcing. This way we find the inertial motion of the system. In this case it is possible to rescale the equations by setting  $\mathbf{X}' = Pr\mathbf{X}$  and  $f' = Prf$  and afterwards dropping the primes. This way we get rid of  $Pr$ . Rescaling a second time we also can take  $f = 1$  by setting  $\mathbf{L}' = f^{-1}\mathbf{L}$ ,  $\mathbf{X}' = f^{-2}\mathbf{X}$  and  $t' = ft$  and again dropping the primes. Ignoring the diffusion, viscosity and forcing terms in (4) and (5) we find after rescaling:

$$\dot{L}_1 + L_3 = -Y \tag{6}$$

$$\dot{L}_2 = X \tag{7}$$

$$\dot{L}_3 - L_1 = 0 \tag{8}$$

$$\dot{X} + YL_3 - ZL_2 = 0 \tag{9}$$

$$\dot{Y} + ZL_1 - XL_3 = 0 \tag{10}$$

$$\dot{Z} + XL_2 - YL_1 = 0 \tag{11}$$

From these rescaled equations we find three different invariants that will help us in our study of the behaviour of the centre-of-mass in the equatorial basin. To find these invariants we look for expressions of which the time derivative is zero, since then way the expression itself has to be constant.

The first expression of which the time derivative is zero, we obtain by adding  $L_1$  times (6),  $L_2$  times (7),  $L_3$  times (8) to (11). This way we find  $\dot{Z} + L_1\dot{L}_1 + L_2\dot{L}_2 + L_3\dot{L}_3 = 0$  and the corresponding invariant is:

$$Z + \frac{1}{2}(L_1^2 + L_2^2 + L_3^2) = c_1 \quad (12)$$

We can consider this as the *conservation of energy*. That way  $Z$  corresponds to the potential energy due to gravity acting on the centre-of-mass and the kinetic energy is represented by  $\frac{1}{2}(L_1^2 + L_2^2 + L_3^2)$ . When there is no external forcing, nor diffusion or viscosity these are the only two terms contributing to the total energy. So the total energy is conserved according to (12).

The second invariant we find by adding  $X$  times (9),  $Y$  times (10) and  $Z$  times (11). This yields  $X\dot{X} + Y\dot{Y} + Z\dot{Z} = 0$ , which corresponds to:

$$X^2 + Y^2 + Z^2 = c_2^2 \quad (13)$$

This conserved quantity shows that in this rough approximation the distance of the centre-of-mass to the geometrical centre is constant. This is due to the absence of diffusion and viscosity. Their presence would cause mixing of the water. When for example the warmest water is at the surface of the basin, and the coldest at the bottom, the centre-of-mass will be located below the geometrical centre of the basin ( $\mathbf{X} = 0$ ). Diffusion would change this and bring the centre-of-mass upwards. In its absence the centre-of-mass will stay at a constant distance from the origin, which is a very strict limitation on the way the water masses can move. Thus this invariant corresponds to the *conservation of stratification*, meaning the water does not mix. All the water will move together with the centre-of-mass.

The last conserved quantity is found by adding  $X$  times (6),  $Y$  times (7),  $Z$  times (8),  $L_1$  times (9),  $L_2 + 1$  times (10) and  $L_3$  times (11). We then find  $X\dot{L}_1 + L_1\dot{X} + Y\dot{L}_2 + (L_2 + 1)\dot{Y} + Z\dot{L}_3 + L_3\dot{Z} = 0$ , corresponding to:

$$XL_1 + YL_2 + ZL_3 + Y = c_3 \quad (14)$$

This invariant says that when the distance of the centre-of-mass to the rotation axis becomes larger, the rotation of the water will slow down and it will speed up when the distance gets smaller. We can write this invariant as  $(f\mathbf{j} + \mathbf{L}) \cdot \mathbf{X}$ , which can be seen as the analogue of potential vorticity. Vorticity is the local rotating motion of a fluid near a certain point [7]. Potential vorticity is defined as  $(\mathbf{f} + \boldsymbol{\omega}) \cdot \frac{\nabla\theta}{\rho}$ , where  $\mathbf{f}$  represents the rotation of the earth,  $\boldsymbol{\omega}$  the relative vorticity of the water (as measured on earth),  $\rho$  the mass density and  $\theta$  the potential temperature [8]. We thus consider this quantity as the *conservation of potential vorticity* (Figure 4).

In principle it is possible to reduce the set of six first order differential equations to a set of three equations using these three invariants. To do so we have to eliminate three of the six variables using the invariants. There are different ways to do this. The first way is set out in Appendix A. Here we



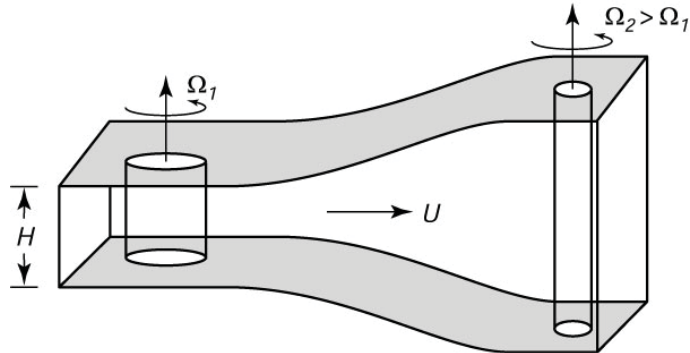


**Figure 4:** A sketch of the conservation of potential vorticity. Stretching of the column of water, corresponding with the centre-of-mass getting closer to the geometrical centre, causes the column to rotate faster. [9]

change to polar coordinates for  $\mathbf{X}$  and cylindrical coordinates for  $L_1$  and  $L_3$  to reduce the number of equations. Another option is to keep the same coordinates and write  $\mathbf{X}$  as a function of  $\mathbf{L}$ . Both ways do not yield ‘nice’ expressions, so we will not look into more detail at this.

In Sections 3.1 and 3.2 we will consider the motion of the centre-of-mass and the angular momentum for certain initial conditions. We will choose the initial conditions in such a way that the equations are (almost) analytically solvable. We use *Mathematica* to compute and visualize the trajectories. By looking at those simple situations we know how the dynamics are when few processes are involved. This will help us to understand the more difficult situations considered in Sections 5 and 6.

### 3.1 A well-mixed state

We first consider the ocean being in a well-mixed state, meaning all mass is equally distributed over the basin. Then the centre-of-mass is located at the geometrical centre of the basin ( $\mathbf{X} = 0$ ). This way also the derivatives of  $X$ ,  $Y$  and  $Z$  are zero, so the centre-of-mass will stay at the origin. The only dynamics in this case is due to the angular momentum and is described by:

$$\dot{L}_1 + L_3 = 0 \tag{15}$$

$$\dot{L}_2 = 0 \tag{16}$$

$$\dot{L}_3 - L_1 = 0 \tag{17}$$

From (16) we conclude that there is a constant rotation around the  $y$ -axis ( $L_2$ ). By combining (15) and (17) we find for  $L_1$  a second order differential equation:

$$\ddot{L}_1 = -L_1 \tag{18}$$

Solving this differential equation yields a periodic solution for  $L_1$ :

$$L_1(t) = A \cos(t + \alpha) \tag{19}$$

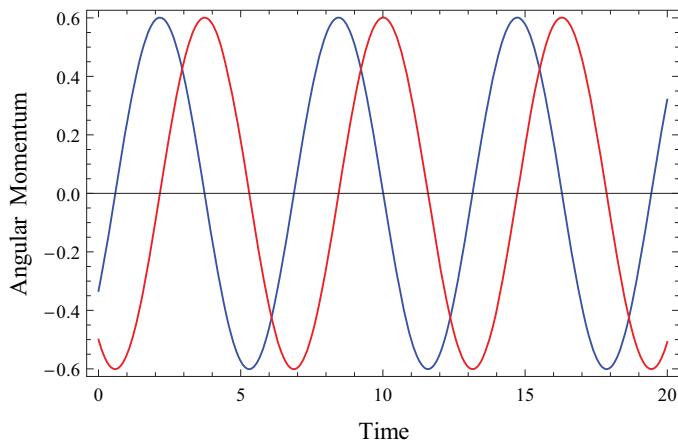


**Figure 5:** The oscillations of  $L_1$  (blue) and  $L_3$  (red) for  $L_1(0) = -1/3$  and  $L_3(0) = -1/2$ .

Here  $A$  and  $\alpha$  depend on the initial situation of the system. Thus we find an inertial oscillation in  $L_1$  and  $L_3$ , since  $L_3 = -\dot{L}_1 = A \sin(t + \alpha)$ . Here  $L_3$  is a quarter of a phase behind  $L_1$ , as can be seen in Figure 5. This holds for all possible initial conditions. Note that before rescaling, taking  $f = 1$ , the Coriolis parameter was in front of the  $L_1$  and  $L_3$  terms. As solving the differential equation (18) yields an oscillation of  $L_1$ , the Coriolis parameter (squared) would in that case determine the period.

So when the basin is in a well-mixed state we find a constant rotation parallel to the equatorial plane ( $L_2$ ). Also we find oscillating angular momenta perpendicular to this plane ( $L_1, L_3$ ) with equal (initial) period and a phase difference of a quarter. The Coriolis force on the equator is the reason this oscillation of  $L_1$  and  $L_3$  takes place. It provides the period of these oscillations and so determines the complete behaviour of the currents in the basin in this situation. Due to the non-conventional Coriolis force the oscillation of the angular momentum is in the  $L_1$  and  $L_3$  part (perpendicular to the equatorial plane) instead of the  $L_1$  and  $L_2$  part (perpendicular to the  $z = 0$  plane), as is the case in the f-plane approximation [4].

### 3.2 Oscillations in the equatorial plane

Another interesting situation is when there is no motion perpendicular to the equatorial plane ( $L_1 = L_3 = 0$ ), nor density difference in this direction ( $Y = 0$ ). Since the time derivatives of  $Y$ ,  $L_1$  and  $L_3$  are in that case also zero,  $Y$ ,  $L_1$  and  $L_3$  will remain zero. The result is that the dynamics is restricted to the equatorial plane. In this case we find a set of three differential equations for  $X$ ,  $Z$  and  $L_2$ :

$$\dot{L}_2 = X \tag{20}$$

$$\dot{X} - ZL_2 = 0 \tag{21}$$

$$\dot{Z} + XL_2 = 0 \tag{22}$$

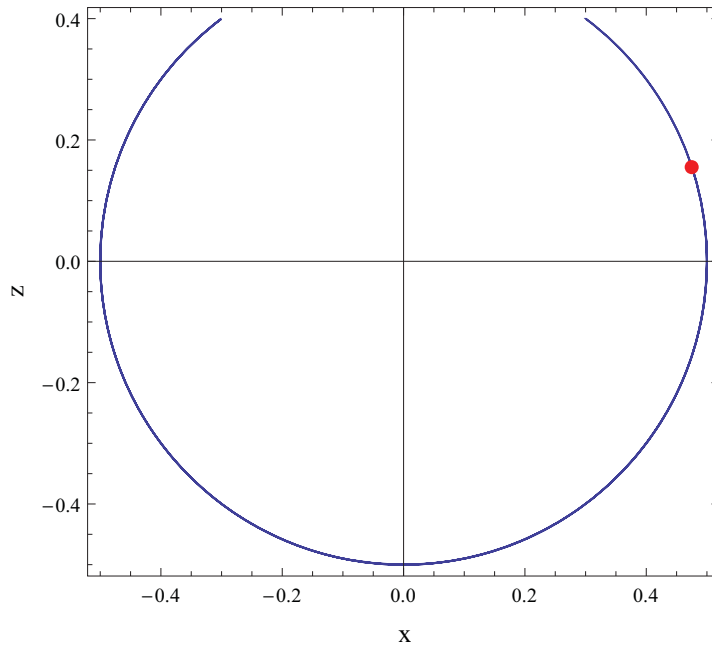


**Figure 6:** The trajectory of the centre-of-mass for  $R = 0.5$ ,  $\phi(0) = \frac{2}{5}\pi$  and  $L_2(0) = 0.7$ . The red dot depicts the initial location of the centre-of-mass.

Here  $X^2 + Z^2 = R^2$  is invariant (as in (13)) and corresponds to the conservation of stratification in the equatorial plane. Using this we change to polar coordinates  $R$  (constant) and  $\phi$  for  $X$  and  $Z$ :

$$X = R \sin \phi \quad Z = R \cos \phi \quad (23)$$

Rewriting (21) (or (22)) using this new coordinates we find a differential equation for  $\phi$ :

$$\dot{\phi} = L_2 \quad (24)$$

Combining the above with (20) results in a second order differential equation in  $\phi$ :

$$\ddot{\phi} = R \sin \phi \quad (25)$$

This differential equation is that of a simple pendulum. For small angles  $\phi$  around  $\phi = \pi$  we have in approximation  $\sin \phi \approx -\phi$ . The corresponding solution is  $\phi(t) = B \cos(\sqrt{R}t + \delta)$ , where  $B$  and  $\delta$  depend on the initial conditions. So for angles  $\phi$  close to  $\pi$ , corresponding to  $X \approx 0$  and  $Z \approx -R$ , there is an oscillation of the centre-of-mass in the equatorial plane with a period proportional to  $R^{-1/2}$ .

To solve the equation for larger angles, we can simplify the equation by multiplying both sides with  $\dot{\phi}$  and reducing. The result is a first order differential equation, which can be solved numerically and analytically (using elliptic integrals [10]):

$$\dot{\phi} = \sqrt{c - 2R \cos \phi} \quad (26)$$

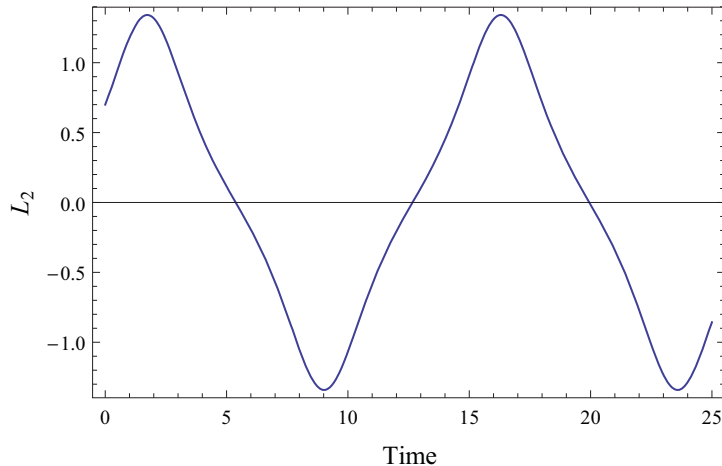


**Figure 7:** The oscillation of  $L_2$  for  $R = 0.5$ ,  $\phi(0) = \frac{2}{5}\pi$  and  $L_2(0) = 0.7$ .

Here  $c$  is a constant to be determined by the initial conditions. In Figure 6 a numerically computed trajectory of the centre-of-mass is shown and in Figure 7 the corresponding graph for  $L_2$  is shown. Depending on the initial conditions there are three different options for the movement of the centre-of mass.

The first option occurs when  $L_2(0) = 0$ . Then the centre-of-mass will oscillate in the equatorial plane around  $(0, -R)$  and every time return to the starting point, but never exceed it. This is due to the conservation of energy. The second option we find when  $0 < L_2(0)^2 < 2R(1 - \cos \phi(0))$ . In that case there is enough energy for the centre-of-mass to exceed its initial position, but not enough to make a full circle as there is still more energy at  $(0, R)$ . In Figure 6 and 7 an example of such an oscillation is shown. The last option occurs when  $L_2(0)^2 > 2R(1 - \cos \phi(0))$ . Now the centre-of-mass will start librating, since there is enough energy to get through the top point.

When in the initial situation the centre-of-mass is located at the equator and there are only currents parallel to the equatorial plane, it will remain this way. We find oscillations of the centre-of-mass in the equatorial plane. The time scale involved is proportional to  $R^{-1/2}$ , meaning that when the distance of the centre-of-mass to the origin increases the time scale decreases. The oscillation will be faster. This inertial oscillation might be an important component of the El Niño-La Niña oscillation. Strengthening or weakening of  $L_2$  affects the height the centre-of-mass reaches. As the location of the centre-of-mass indicates density differences, and thus possibly temperature differences, in the equatorial plane, changes in this oscillation can lead to an El Niño or La Niña. The question now is which (periodic) forcings affect the angular momentum  $L_2$ .

## 4 Ignoring diffusion and viscosity

To see what happens when the inertial system is forced we include forcings due to buoyancy fluxes. We still ignore diffusion, viscosity and wind. This way we find another set of equations. In these equations we have scaled out  $Pr$  and  $f$

in the same way as in Section 3. Furthermore we have rescaled  $\mathbf{F}$  by setting  $\mathbf{F}' = PrRa f^2 \mathbf{F}$  and dropping the prime afterwards. This way we also get rid of  $Ra$  and the equations become:

$$\dot{L}_1 + L_3 = -Y \quad (27)$$

$$\dot{L}_2 = X \quad (28)$$

$$\dot{L}_3 - L_1 = 0 \quad (29)$$

$$\dot{X} + YL_3 - ZL_2 = F_1 \quad (30)$$

$$\dot{Y} + ZL_1 - XL_3 = F_2 \quad (31)$$

$$\dot{Z} + XL_2 - YL_1 = F_3 \quad (32)$$

Except for the  $\mathbf{F}$  terms, these equations are the same as in Section 3. In the following we will look at the situation of Section 3.2, but now also take forcing into account. This way we will see what the consequences of forcings are when no damping due to diffusion and viscosity takes place.

#### 4.1 Forced oscillations in the equatorial plane

We again look at the situation with only motion parallel to the equatorial plane ( $Y = L_1 = L_3 = 0$ ). This time we look at the consequences of different forcing mechanisms. Now if we want  $Y$  to remain zero, it is necessary for  $F_2$  to be zero too. This means there are no buoyancy fluxes in the meridional direction which would force the centre-of-mass out of the equatorial plane. It still remains possible to have buoyancy fluxes in the zonal and vertical directions, which are parallel to the equator. These buoyancy fluxes can for example be due to differential heat input at the east ( $F_1 < 0$ ) or west ( $F_1 > 0$ ) side or at the surface ( $F_3 < 0$ ) or bottom ( $F_3 > 0$ ). The set of equations under these conditions becomes:

$$\dot{L}_2 = X \quad (33)$$

$$\dot{X} - ZL_2 = F_1 \quad (34)$$

$$\dot{Z} + XL_2 = F_3 \quad (35)$$

These equations describe the motion of the centre-of-mass when it is forced by for example differential heating. Due to the forcings it is possible to drive the centre-of-mass to infinity, as there is no damping. Therefore this approximation may not be realistic, but it does show what happens to the centre-of-mass when it is forced in the vertical and zonal direction.

Note that when we add friction to the above equations (meaning (33) becomes  $\dot{L}_2 = X - L_2$ ) and ignore buoyancy fluxes in the zonal direction ( $F_1 = 0$ ) the Diffusionless Lorenz Equations are found [11], [12]. For this equations we know periodic and chaotic solutions exist. In this equations however our non-conventional Coriolis parameter does not play a role for the equilibria. The only difference is the plane in which the dynamics takes place as before.

#### 4.1.1 Vertical differential buoyancy fluxes

First we look at the situation in which there are only buoyancy fluxes in the vertical direction ( $F_1 = 0, F_3 \neq 0$ ). These buoyancy fluxes are due to for example precipitation ( $F_3 < 0$ ) or evaporation ( $F_3 > 0$ ). Here we find an invariant which we can compare with the invariant for conservation of energy:

$$Z + \frac{1}{2}L_2^2 - F_3t = c \quad (36)$$

In this equation  $t$  depicts the time. By inserting (34) into the derivative of (33) and using the above invariant we find a second order differential equation for  $L_2$ . Here we take  $c$  to be zero as it is possible to move the zero of the time. Also we can rescale the equations by taking  $t' = F_3^{1/3}t$  and  $L_2' = F_3^{-1/3}L_2$  and dropping the primes afterwards. This way we find a second order differential equation for  $L_2$ :

$$\ddot{L}_2 = -\frac{1}{2}L_2^3 + tL_2 \quad (37)$$

By using  $L_2' = -\frac{i}{2}L_2$ , this equation changes to  $\ddot{L}_2 = 2L_2^3 + tL_2$ , which is the second Painlevé equation with a solution called the second Painlevé transcendent. A Painlevé transcendent is the solution to a non-linear second-order differential equation in the complex plane [10]. For this equation the points where the solution is not continuous all have to be poles, which means that as we approach such a point the solution goes to infinity. The location of these points also depends on the initial conditions.

The consequence is that  $L_2$  keeps growing, meaning the rotation will go ever faster, which is not a physically acceptable solution. This is due to the absence of diffusion and viscosity, which would prevent the forcing from driving  $L_2$  to infinity. This feature can already be deduced from (37). As the time  $t$  keeps increasing,  $Z$  and/or  $L_2$  have to keep increasing as well (in absolute value).

In the situation of differential heat input at the surface by solar radiation ( $F_3 < 0$ ) this approximation does not yield acceptable solutions. The constant input of energy makes the angular momentum go to infinity, corresponding to ever faster rotation in the basin. As this is one of the important forcings in the Pacific Ocean, we now know damping is necessary in order to prevent the rotation in the system becomes infinitely large.

#### 4.1.2 Zonal differential buoyancy fluxes

Secondly we look at the situation where only differential buoyancy fluxes in the zonal direction occur ( $F_3 = 0, F_1 \neq 0$ ). This corresponds for example with river input at the east or west side of the basin ( $F_1 < 0, F_1 > 0$  respectively). In this case energy conservation still holds, so  $Z + \frac{1}{2}L_2^2 = c$ . After rescaling by  $t' = \sqrt{c}t$ ,  $L_2' = \frac{1}{2\sqrt{c}}L_2$  and  $F_1' = \frac{F_1}{2c\sqrt{c}}$ , we find a second order differential equation for  $L_2$ :

$$\ddot{L}_2 = -2L_2^3 + L_2 + F_1 \quad (38)$$

Note that the number of degrees of freedom is reduced to two by using the invariant. By multiplying both sides with  $\dot{L}_2$ , we can simplify this equation to a first order differential equation:

$$\dot{L}_2 = \sqrt{-L_2^4 + L_2^2 + 2F_1L_2 + c'} \quad (39)$$

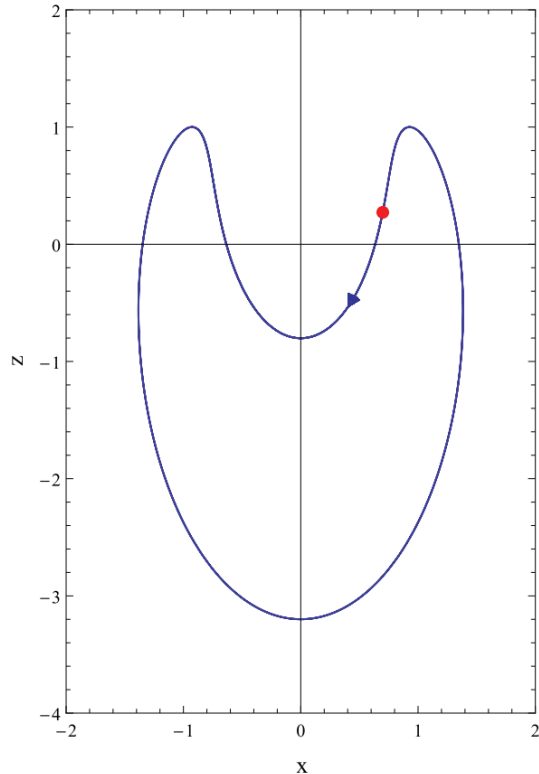


**Figure 8:** The trajectory of the centre-of-mass for  $F_1 = -0.5$ ,  $L_2(0) = 0.6$  and  $\dot{L}_2(0) = 0.7$ . The red dot depicts the initial location of the centre-of-mass and the arrow shows the direction.

Here  $c'$  is a constant determined by the initial conditions. Now we also rescale  $X$  and  $Z$  by setting  $X' = \frac{1}{2c}X$  and  $Z' = \frac{1}{c}Z$  and dropping the primes afterwards. This way we find in the rescaled coordinates  $X = L_2$  and  $Z = 1 - 2L_2^2$ . In Figure 8 a trajectory of the centre-of-mass according to these equations is shown. In Figure 9 the corresponding graph for  $L_2$  is depicted.

As in Section 3.2 we can distinguish three different situations for the movement of the centre-of-mass. The first is where  $L_2(0) = 0$ . In this case the centre-of-mass will never exceed its initial position due to energy conservation. The form of the trajectory will change for different forcing strengths. When  $F_1$  is large in absolute value the trajectory is almost flat at the top, but there still is a small dip where  $L_2$  changes sign causing the centre-of-mass not to exceed its initial location.

The second option is when the centre-of-mass does exceed its initial position, but does not make a circle-like movement. This case is shown in Figures 8 and 9. We can compare this to the oscillation found in Section 3.2, only this time the clockwise and counterclockwise paths differ. The last case is when it does make a circle-like movement, so there is no dip any more in the path at  $x = 0$ . This is comparable to the case in Section 3.2 where the centre-of-mass makes a full circle.

The presence of differential heating in the zonal direction does change the behaviour of the system at the equator. When we compare the situation where this forcing is present with the situation without (Section 3.2) the largest difference is the path of the centre-of-mass. The distance to the geometrical centre is no longer conserved and thus the clockwise and counterclockwise paths do not have to be the same any more. Only forcing in the zonal direction does not drive  $L_2$  to infinity in contrast to forcing in the vertical direction ( $F_3$ ). This is possibly due to gravity, which works in the same direction as  $F_3$ .

In the Pacific Ocean there is a temperature difference between the east and west side of the basin. Considering this as a forcing mechanism, it changes the inertial oscillation. When this forcing increases in strength, the upper minimum gets closer to the maxima (Figure 8). We thus see zonal buoyancy fluxes affect the angular momentum in the equatorial plane ( $L_2$ ). It changes the shape of the oscillation in  $L_2$ , but does not affect its period. During El Niño the temperature difference in the zonal direction increases. The magnitude of the deviation from the inertial movement due to  $F_1$  could provide information about the strength of El Niño.

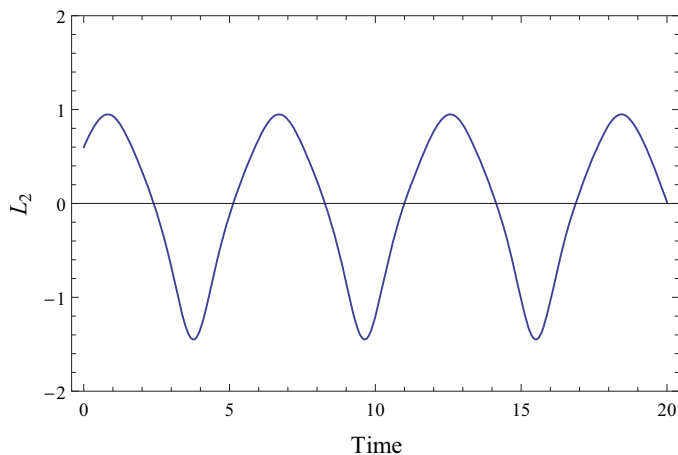


**Figure 9:** The oscillation of  $L_2$  for  $F_1 = -0.5$ ,  $L_2(0) = 0.6$  and  $\dot{L}_2(0) = 0.7$ .

## 5 Dominant mixing of momentum

In the previous sections we did not take friction and diffusion into account. There were no sinks of energy. In this section we add both friction and diffusion and consider the case where  $Pr \rightarrow \infty$ . This means the mixing of momentum in the basin happens fast compared to the mixing of temperature and salt. Viscosity is thus more important than diffusion. In this case (4) simplifies to:

$$fL_3 = -Y - L_1 + T_1 \quad (40)$$

$$0 = X - L_2 + T_2 \quad (41)$$

$$-fL_1 = -rL_3 + T_3 \quad (42)$$



Here we have rescaled  $\mathbf{T}$  by setting  $\mathbf{T}' = \hat{T}\mathbf{T}$  and dropping the prime. From these equations we can find the angular momenta  $L_1$ ,  $L_2$  and  $L_3$  as functions of  $X$ ,  $Y$  and  $Z$ . For  $L_2$  we only need to rewrite (41) to find:

$$L_2 = X + T_2 \quad (43)$$

To find  $L_1$  and  $L_3$  it is necessary to combine (40) and (42). This way we find:

$$L_1 = \frac{-rY + rT_1 - fT_3}{f^2 + r} \quad (44)$$

$$L_3 = \frac{-fY + fT_1 + T_3}{f^2 + r} \quad (45)$$

Substituting these in (5) yields three ordinary differential equations for the centre-of-mass  $\mathbf{X}$ :

$$\dot{X} + Y(-bY + d) - Z(X + T_2) = -X + F_1 \quad (46)$$

$$\dot{Y} + Z(-aY + c) - X(-bY + d) = -Y + F_2 \quad (47)$$

$$\dot{Z} + X(X + T_2) - Y(-aY + c) = -\mu Z + F_3 \quad (48)$$

Here  $a = \frac{r}{f^2+r}$ ,  $b = \frac{f}{f^2+r}$ ,  $c = \frac{rT_1-fT_3}{f^2+r}$  and  $d = \frac{fT_1+T_3}{f^2+r}$ . The equilibrium points  $\mathbf{X}_0$  of these equations, for which  $\dot{\mathbf{X}}_0 = 0$ , are the intersection points of three surfaces defined by these equations. The first surface is an *ellipsoid* found by adding  $X_0$  times (46),  $Y_0$  times (47) and  $Z_0$  times (48):

$$(X_0 - \frac{1}{2}F_1)^2 + (Y_0 - \frac{1}{2}F_2)^2 + \mu(Z_0 - \frac{1}{2\mu}F_3)^2 = \frac{1}{4}(F_1^2 + F_2^2 + \frac{1}{\mu}F_3^2) \quad (49)$$

The location of the centre of this ellipsoid is determined by the buoyancy fluxes  $\mathbf{F}$ , as is the length of its axes. Since the axes in the zonal and meridional direction are of equal length, this is an ellipsoid of revolution. This means it can be formed by revolving an ellipse in a plane perpendicular to the  $x$ - $y$ -plane around its central  $z$ -axis. The parameter  $\mu$ , being the diffusion-ratio, determines the ratio between the two horizontal axes and the vertical one. This difference is thus caused by the difference in diffusion between the horizontal and vertical direction.

This surface can be compared to the second invariant (13) in Section 3. This invariant corresponds to the conservation of stratification. The surface thus gives some information about the stratification of the basin in equilibrium. Depending on the strength and direction of the buoyancy fluxes, the system wants to reach a situation of stratification around a certain point.

The second surface is a *paraboloid* which we find by rearranging (48):

$$(X_0 + \frac{T_2}{2})^2 + a(Y_0 - \frac{c}{2a})^2 = F_3 + \frac{T_2^2}{4} + \frac{c^2}{4a} - \mu Z_0 \quad (50)$$

Since  $a > 0$  this is an elliptic paraboloid. Also the paraboloid has a maximum since we have a minus sign in front of  $Z_0$ . The  $x$ - and  $y$ -coordinate of this maximum are determined only by the differential momentum fluxes ( $T_1$ ,  $T_2$  and  $T_3$ ), whereas the  $z$ -coordinate is also dependent on vertical buoyancy fluxes ( $F_3$ ).

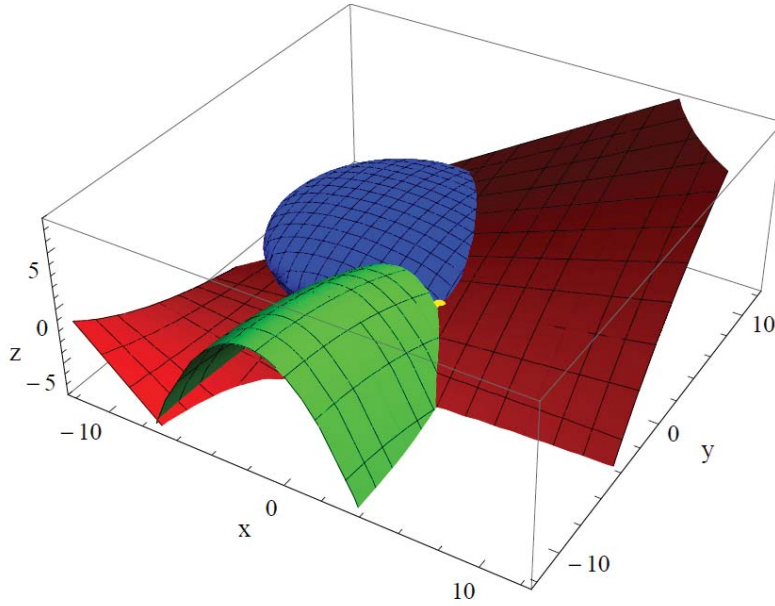


**Figure 10:** The surfaces where  $\dot{\mathbf{X}} = 0$  with the ellipsoid in blue, the paraboloid in green and the surface of (51) in red for  $\mu = 3$ ,  $f = 5$ ,  $r = 2$ ,  $F_1 = -9$ ,  $F_2 = 9$ ,  $F_3 = -10$ ,  $T_1 = -5$ ,  $T_2 = 4$  and  $T_3 = 9$ . One of the equilibrium points is shown in yellow.

As a consequence there are situations where the ellipsoid is completely above the paraboloid in which there are no equilibrium points. Similarly there are situations where the ellipsoid lies completely under the paraboloid.

In a way we can compare this surface to the first invariant (12) in Section 3 which corresponds to the conservation of energy. As  $X$  and  $Y$  can be written as functions of the angular momentum, the left side of (50), together with  $-\frac{T_2^2}{4} - \frac{c^2}{4a}$ , represents the kinetic energy in equilibrium. On the right side  $F_3 - \mu Z_0$  corresponds to gravitational energy.

The last surface is most difficult to visualise. It is found by rearranging (47). This way we find an equation for  $Y_0$  as a function of  $X_0$  and  $Z_0$ <sup>1</sup>:

$$Y_0 = \frac{cZ_0 - dX_0 - F_2}{aZ_0 - bX_0 - 1} \quad (51)$$

When the denominator is zero, also the numerator has to be zero, so there will be only one line where this is the case (all values for  $Y_0$  are possible). When the denominator is not zero,  $Y_0$  will go asymptotically to plus or minus infinity (depending on  $cZ_0 - dX_0 - F_2$  being positive or negative) as  $X_0$  and  $Z_0$  approach the line  $aZ_0 - bX_0 - 1 = 0$ .

All three surfaces are shown in Figure 10 for certain values of the parameters. The points where all three surfaces intersect are the equilibrium points (not

<sup>1</sup>There exists a surface which corresponds to the conservation of potential vorticity (14), but it is even harder to visualise.

necessarily stable). The locations of these points depend on the values of the parameters. Since it is very hard to compute the stable points analytically taking all parameters into account, it is easier to compute them numerically. Then, however, values of all parameters have to be given. Because there is a large uncertainty in most (if not all) parameters, we will in the following sections look at cases where we can find the equilibrium points exactly. This is done by keeping at most one forcing parameter and setting the others to zero.

## 5.1 Without forcing

First we look at the situation without any forcing mechanisms. When this is the case the equations are:

$$\dot{X} - bY^2 - ZX = -X \quad (52)$$

$$\dot{Y} - aZY + bXY = -Y \quad (53)$$

$$\dot{Z} + X^2 + aY^2 = -\mu Z \quad (54)$$

Now we want to find the equilibrium points for which  $\dot{\mathbf{X}}_0 = 0$ . When  $Y = 0$  it will remain this way, since then  $\dot{Y} = 0$ . For a fixed point with  $Y_0 = 0$  we find the values for  $X_0$  and  $Z_0$  by solving (52) and (54). The solutions are  $Z_0 = 0$  and  $X_0 = 0$  or  $Z_0 = 1$  and  $X_0 = \pm i\sqrt{\mu}$ . The last options however are imaginary as  $\mu$  is always positive and so do not represent physical solutions. So the geometrical centre is an equilibrium point.

Other fixed points are found when  $aZ - bX = 1$ , since then too  $\dot{Y} = 0$ . In this case however, we can not set  $Y_0$  to zero, as (52) and (54) have to be satisfied as well. For  $X_0$  and  $Z_0$  we now find:

$$X_0 = \frac{-\mu b}{a(a-1) + \mu b^2} \quad Z_0 = \frac{a-1}{a(a-1) + \mu b^2} \quad (55)$$

For the corresponding  $Y_0$ -values it has to hold that:

$$Y_0^2 = \frac{-\mu((a-1)^2 + \mu b^2)}{(a(a-1) + \mu b^2)^2} \quad (56)$$

This means  $Y_0^2$  will always be negative as  $\mu$  is always positive. Therefore this also yields imaginary values and so gives non-physical solutions. Thus in the case there is no forcing we find only the origin as an equilibrium point. To see if it is stable we compute the Jacobian matrix at this fixed point:

$$J = \begin{pmatrix} \frac{\partial \dot{X}}{\partial X} & \frac{\partial \dot{X}}{\partial Y} & \frac{\partial \dot{X}}{\partial Z} \\ \frac{\partial \dot{Y}}{\partial X} & \frac{\partial \dot{Y}}{\partial Y} & \frac{\partial \dot{Y}}{\partial Z} \\ \frac{\partial \dot{Z}}{\partial X} & \frac{\partial \dot{Z}}{\partial Y} & \frac{\partial \dot{Z}}{\partial Z} \end{pmatrix}_{(0,0,0)} = \begin{pmatrix} -1 & 0 & 0 \\ 0 & -1 & 0 \\ 0 & 0 & -\mu \end{pmatrix} \quad (57)$$

The eigenvalues of this matrix are  $-1$  (two times) and  $-\mu$ . These are all negative, hence the origin is a stable equilibrium point.

Now we want to know whether the centre-of-mass will always end up at the geometrical centre, no matter where it is at  $t = 0$ . To investigate this we look at a sphere of radius  $r$  centred at the origin. The direction of the outer-pointing normal  $\mathbf{n}$  is  $(x_n, y_n, z_n)$  for every point  $(x_n, y_n, z_n)$  on the sphere. Calculating

the dot product of  $\mathbf{n}$  with the vector field determined by  $\dot{\mathbf{X}}$  at the same point yields  $-(x_n^2 + y_n^2 + \mu z_n^2)$ , which is always negative (for  $x_n, y_n, z_n \neq 0$ ). The dot product being negative means that the vector field on the sphere always points inwards, no matter what the radius is. Since this holds for every possible  $r$ , the centre-of-mass will always move towards the centre of the basin, no matter where it starts.

Physically this is quite obvious. Due to the presence of viscosity all movement in the system will be damped. And due to diffusion the mass will become equally distributed through the basin. As there are no forcings to oppose these effects, the centre-of-mass will end up at the geometrical centre. Also the rotation in the basin will go to zero, as can also be seen in (43), (44) and (45).

In reality most basins are of course forced by all sort of mechanisms. Now we know the behaviour of the basin when no forcing takes place we will look at the influence of some forcing mechanisms separately. The final purpose is to see if including few forcings might result in periodic behaviour corresponding to the El Niño-La Niña oscillation.

## 5.2 Equatorial symmetric forcings

By setting some of the differential momentum and buoyancy fluxes to zero the differential equations simplify making it easier to find the equilibrium points. This happens when only forcings which are symmetric in the equator are kept ( $T_1 = T_3 = F_2 = 0$ ). This means there are no differential buoyancy fluxes in the meridional direction ( $F_2$ ). Also we ignore wind torque at the surface ( $T_3$ ) and wind in the meridional direction ( $T_1$ ). We still have the possibility for wind in the zonal direction ( $T_2$ , the trades). Moreover differential buoyancy fluxes in the vertical ( $F_3$ ) and zonal direction ( $F_1$ ) remain possible. These forcing parameters are quite realistic for an ocean basin on the equator (see Section 1). Under these conditions (46), (47) and (48) simplify to:

$$\dot{X} - bY^2 - Z(X + T_2) = -X + F_1 \quad (58)$$

$$\dot{Y} - aYZ + bXY = -Y \quad (59)$$

$$\dot{Z} + X(X + T_2) + aY^2 = -\mu Z + F_3 \quad (60)$$

Since we can write (59) as  $\dot{Y} = Y(aZ - bX - 1)$  this yields two possibilities for the fixed points ( $\dot{\mathbf{X}}_0 = \mathbf{0}$ ):

1.  $Y_0 = 0$
2.  $aZ_0 - bX_0 = 1$

Based on these two options we can divide the equilibrium dynamics into two parts. One part which is symmetric in the equatorial plane ( $Y_0 = 0$ ) and another part which is not ( $aZ_0 - bX_0 = 1$ ). The symmetric part is expected as all forcings we take into account act parallel to the equatorial plane. The equilibrium dynamics which are not symmetric are more surprising. As the forcings above the equator are in approximation mirror symmetric in the equatorial plane, this is a quite realistic situation.

In the equatorial symmetric case (58) and (60) (for  $\dot{X} = \dot{Z} = 0$ ) lead to a cubic equation in  $X_0$  (or  $Z_0$ ), which can be solved analytically. This results in three fixed points for which we have to check if they are real.

In the asymmetric case  $X_0$  and  $Z_0$  are linearly related. The solutions for  $X_0$  and  $Z_0$  in this case are:

$$X_0 = \frac{-\mu b + a(T_2 + aF_1 + bF_3)}{a(a-1) + \mu b^2} \quad Z_0 = \frac{a-1 + b(T_2 + aF_1 + bF_3)}{a(a-1) + \mu b^2} \quad (61)$$

Knowing the values of  $X_0$  and  $Z_0$ , there is a linear equation in  $Y_0^2$  left to solve. This gives two possible values  $\pm Y_0$ , which are real under certain conditions. In that case we find two off-equatorial fixed points. In the following we will look at the influence of each forcing parameter separately, since otherwise the equations to solve remain very complicated.

### 5.2.1 Zonal winds

First we look at the case where only differential momentum fluxes in the zonal direction are present ( $T_2 \neq 0$ ,  $F_1 = F_3 = 0$ ). This corresponds with wind to the west ( $T_2 < 0$ ) or east ( $T_2 > 0$ ). In this section we will first compute all equilibrium points. Next we will investigate their stability by computing the eigenvalues of the Jacobian matrix. Finally we will look if the centre-of-mass will always move towards one of these fixed points (or the one fixed point) by searching for a surface for which the vector field of  $\dot{\mathbf{X}}$  points inwards for every possible size of this surface.

We first compute the equilibrium points in the equatorial plane ( $Y_0 = 0$ ). Solving the corresponding cubic equation yields  $(0, 0, 0)$ ,  $(-i\sqrt{\mu} - T_2, 0, 1 - \frac{iT_2}{\sqrt{\mu}})$  and  $(i\sqrt{\mu} - T_2, 0, 1 + \frac{iT_2}{\sqrt{\mu}})$  as fixed points. The last two are not real as  $\mu > 0$  and therefore only the origin is a physically acceptable fixed point.

For the fixed points outside the equatorial plane it is necessary for  $Y_0^2$  to be positive. With only  $T_2$  we have:

$$Y_0^2 = \frac{-(a^2 + \mu b^2)T_2^2 + 2\mu bT_2 - \mu((a-1)^2 + \mu b^2)}{(a(a-1) + \mu b^2)^2} \quad (62)$$

This is a parabola in  $T_2$  with a maximum (as the term in front of  $T_2^2$  is negative). If this maximum is smaller than zero, there are no points where  $Y_0^2$  is positive and as a consequence there are no real solutions. To see if this is the case we solve  $Y_0^2 = 0$  for  $T_2$ . This results in:

$$T_2 = \frac{\mu b \pm i\sqrt{\mu}|a(a-1) + \mu b^2|}{a^2 + \mu b^2} \quad (63)$$

Thus we find no real solutions, as  $\mu > 0$ , except when  $a(a-1) = -\mu b^2$ . In that case however the value of  $Y_0^2$  is undetermined, since the denominator is zero. We conclude there are no equilibrium points outside the equatorial plane. So only the geometrical centre is a fixed point when we have zonal differential buoyancy fluxes.

We have found only the origin as an equilibrium point. Now we check if it is stable, as is the case when  $T_2 = 0$  (Section 5.1). To investigate this, we compute the Jacobian matrix:

$$J = \begin{pmatrix} -1 & 0 & T_2 \\ 0 & -1 & 0 \\ -T_2 & 0 & -\mu \end{pmatrix} \quad (64)$$

To find the eigenvalues we diagonalise this matrix and this gives  $-1$ ,  $-1$  and  $-\mu - T_2^2$ . Again all of these are always negative so we conclude that the origin is again a stable point. Showing the centre-of-mass will always move towards the geometrical goes in exactly the same way as in Section 5.1. The dot product again yields  $-(x_n^2 + y_n^2 + \mu z_n^2)$ , so indeed the centre-of-mass will always move towards the geometrical centre.

The presence of wind in the zonal direction does change the behaviour of the system. It does not change the fact the centre-of-mass will end up at the geometrical centre, but it does change the path it follows towards the geometrical centre. What it also changes is the angular momentum. According to (43), (44) and (45) we find  $\mathbf{L} = (0, T_2, 0)$ , meaning there is a rotation of magnitude  $T_2$  around the  $y$ -axis.

Physically this means all rotation in the basin is damped until only the rotation forced by the zonal winds ( $L_2$ ) remains. The density distribution in that case will be homogeneous as the rotation does not change the location of the centre-of-mass. So the system is well-mixed.

The trade winds are an important part of the forcings on the equator and in our model correspond to negative  $T_2$ . We have shown that presence of only  $T_2$  yields one stable point at the geometrical where the centre-of-mass will always end up. For periodic behaviour causing El Niño more forcings are needed.

### 5.2.2 Zonal differential buoyancy fluxes

The second situation we consider is when only zonal buoyancy fluxes are present ( $F_1 \neq 0, T_2 = F_3 = 0$ ). This corresponds for example with warm water input at the east (or west) side of the basin ( $F_1 < 0$  or  $F_1 > 0$  respectively). Our approach will be the same as in Section 5.2.1. We will first consider the situation in the equatorial plane ( $Y_0 = 0$ ) and secondly the situation outside this plane ( $aZ_0 - bX_0 - 1 = 0$ ). In the first case the cubic equation again yields one real solution, this time however not the origin, but:

$$X_0 = \frac{\frac{\mu}{3} - \left(\frac{\mu}{18}(-9F_1 + \sqrt{3(27F_1^2 + 4\mu)})\right)^{2/3}}{\left(\frac{\mu}{18}(-9F_1 + \sqrt{3(27F_1^2 + 4\mu)})\right)^{1/3}} \quad (65)$$

$$Z_0 = -\frac{X^2}{\mu} = -\frac{1}{\mu} \frac{\left(\frac{\mu}{3} - \left(\frac{\mu}{18}(-9F_1 + \sqrt{3(27F_1^2 + 4\mu)})\right)^{2/3}\right)^2}{\left(\frac{\mu}{18}(-9F_1 + \sqrt{3(27F_1^2 + 4\mu)})\right)^{2/3}} \quad (66)$$

Together with  $Y_0 = 0$  this gives a fixed point when only  $F_1$  is present. Now we wonder if this point is stable in some cases. Putting  $Y_0 = 0$  (but not yet (65) and (66)) into the Jacobian matrix gives:

$$J = \begin{pmatrix} Z_0 - 1 & 0 & X_0 \\ 0 & aZ_0 - bX_0 - 1 & 0 \\ -2X_0 & 0 & -\mu \end{pmatrix} \quad (67)$$

By diagonalizing this matrix, we find the eigenvalues to be  $Z_0 - 1$ ,  $aZ_0 - bX_0 - 1$  and  $-\mu + \frac{2X_0^2}{Z_0 - 1}$ . Since  $Z_0 = -\frac{X_0^2}{\mu}$ , it follows that always  $Z_0 - 1 < 0$ , so in at least one direction there is stability. For the second value it is more difficult. Again using  $Z_0 = -\frac{X_0^2}{\mu}$ , we find stability when  $-\frac{aX_0^2}{\mu} - bX_0 - 1 < 0$ . Since this is a parabola with a maximum, we can look at the location of the top

to see when this is the case. The maximum value is  $\frac{\mu b^2}{4a} - 1$ , meaning there is always stability when  $\mu b^2 < 4a$ , since then the maximum is negative. However, as  $X_0$  is a function of  $F_1$ , there are also certain values of  $F_1$  for which stability is found when  $\mu b^2 \geq 4a$ . For stability we need  $X_0$  to be outside:

$$X_0 = \frac{-\mu b \pm \sqrt{\mu(\mu b^2 - 4a)}}{2a} \quad (68)$$

This corresponds with  $F_1$  being outside:

$$F_1 = \frac{-\mu b(\mu b^2 + a(a-3)) \pm (\mu b^2 + a(a-1))\sqrt{\mu(\mu b^2 - 4a)}}{2a^3} \quad (69)$$

For such values of  $F_1$  we find stability in the meridional direction. The last eigenvalue again is always negative. Because  $Z_0 - 1 < 0$ , we have  $\frac{2X_0^2}{Z_0-1} < 0$ . This leads again to stability in the vertical direction.

So when  $\mu b^2 < 4a$  all eigenvalues are negative for all possible zonal differential buoyancy fluxes and thus the equilibrium point in the equatorial plane is stable. When this is not the case, there is instability in the meridional direction for certain values of  $F_1$  (outside the interval of (69)), but nevertheless stability in the other directions.

Next we look at the equilibrium points outside the equatorial plane ( $aZ_0 - bX_0 - 1 = 0$ ). Here we need  $Y_0^2$  to be positive as in the previous sections. Now we have:

$$Y_0^2 = -\frac{a^3 F_1^2 + \mu b(a(a-3) + \mu b^2)F_1 + \mu((a-1)^2 + \mu b^2)}{(a(a-1) + \mu b^2)^2} \quad (70)$$

To see if this is positive, we solve  $Y_0^2 = 0$  for  $F_1$  as in Section 5.2.1 has been done for  $T_2$ . In this case we find again (69). This is real only when  $\mu b^2 \geq 4a$ . When this holds,  $Y_0^2$  is positive when  $F_1$  is in between both values in (69). So there are equilibrium points outside the equatorial plane.

We now focus on the stability of these fixed points. In the same way as in Section 5.2.1 we compute the eigenvalues of the Jacobian matrix at both points. In this case the Jacobian matrix is:

$$J = \begin{pmatrix} Z_0 - 1 & 2bY_0 & X_0 \\ -bY_0 & 0 & aY_0 \\ -2X_0 & -2aY_0 & -\mu \end{pmatrix} \quad (71)$$

After diagonalizing we find  $Z_0 - 1$ ,  $\frac{2b^2 Y_0^2}{Z_0 - 1}$  and  $-\frac{a(a-1) + \mu b^2}{b^2}$  to be the eigenvalues. Again  $Z_0 - 1$  is always negative, since here  $Z_0 = -\frac{X_0^2 + aY_0^2}{\mu}$  (from (60)). Therefore also  $\frac{2b^2 Y_0^2}{Z_0 - 1} < 0$ . Lastly  $-\frac{a(a-1) + \mu b^2}{b^2}$  is negative, as  $\mu b^2 > 4a > a(1-a)$ . Thus when the conditions for having these fixed points are met, they are also stable.

Now we wonder whether the centre-of-mass will always move towards (one of) the equilibrium point(s), no matter where it starts. We examine the different cases separately. First we look at the stable point which is found when  $\mu b^2 < 4a$ . In this case the stable location of the centre-of-mass will be in the equatorial plane for all possible strengths and directions of the zonal buoyancy fluxes ( $F_1$ ).

To see if the centre-of-mass will always go there we first make a translation to ensure that the equilibrium point  $(X_0, 0, Z_0)$  is located at the origin:

$$X \rightarrow X + X_0 \quad Y \rightarrow Y \quad Z \rightarrow Z + Z_0 \quad (72)$$

After this translation we can use the same strategy as in Section 5.1. We compute the dot product of  $\dot{\mathbf{X}}$  with the outer normal of a sphere and find:

$$-x_n^2(1 - Z_0) + y_n^2(aZ_0 - bX_0 - 1) - \mu z_n^2 - X_0 x_n z_n \quad (73)$$

Here we have used that  $X_0(Z_0 - 1) + F_1 = 0$  and  $-X_0^2 - \mu Z_0 = 0$ . Since  $aZ_0 - bX_0 - 1 < 0$  for this equilibrium point it follows that also  $y_n^2(aZ_0 - bX_0 - 1) \leq 0$ , meaning the centre-of-mass will always move towards the equatorial plane. We now want the  $x_n$ - $z_n$ -part of (73) to be also negative for all  $x_n$  and  $z_n$ , as we then know the centre-of-mass always moves towards this fixed point. To investigate if this is the case we remove  $y_n^2(aZ_0 - bX_0 - 1)$  from (73) and write it as:

$$-x_n^2 - \frac{3}{4}\mu z_n^2 - \left(\frac{X_0}{\sqrt{\mu}}x_n + \frac{\sqrt{\mu}}{2}z_n\right)^2 \quad (74)$$

This is always negative. So in the case  $\mu b^2 < 4a$  we find for all points on a sphere that, no matter the radius, the centre-of-mass will always move inwards. Wherever the centre-of-mass starts, it will always move towards the equilibrium point in the equatorial plane. Also when  $\mu b^2 > 4a$  and  $F_1$  outside the interval of (69) the centre-of-mass will move inward. In both situations the angular momentum in equilibrium will be  $(0, X_0, 0)$ , so there will be rotation around the  $y$ -axis of order  $X_0$ .

Secondly we have to look at what happens when  $\mu b^2 > 4a$  and  $F_1$  inside the interval of (69). Graphs (Figure 11) suggest that when the centre-of-mass starts somewhere outside the equatorial plane it will always move towards the stable point at its side of the this plane. It is however very hard to proof this. A sphere, as in Section 5.1, does not work, nor does a cylinder around the line between the two stable points. Which surface does work has to be investigated.

We have found that in presence of only zonal differential buoyancy fluxes there is always a stable point in the equatorial plane when  $\mu b^2 < 4a$ . This condition corresponds with the diffusion-ratio being smaller than the friction-ratio. For  $\mu b^2 > 4a$  there are still fixed points in this plane, which are stable under the condition  $F_1$  is outside the interval of (69). The angular momentum will in this case be  $(0, X_0, 0)$ , so there is only rotation around the  $y$ -axis. This is expected as for example heating at the east side causes a density difference between east and west and thus initiates rotation in this direction.

When  $\mu b^2 > 4a$  and  $F_1$  is inside the interval of (69) new stable points are found outside the equatorial plane. These are more surprising than the ones in the equatorial plane, as the symmetry of the equator is broken. This happens when the diffusion-ratio is larger than the friction-ratio. Another condition is that  $F_1$  is negative which corresponds with differential heat input at the east side of the basin.

During an El Niño the temperature difference between east and west lowers. If this is due to extra heat input at the east side, this causes the centre-of-mass to move towards the origin (smaller  $X_0$ ). If this forcing is strong enough it



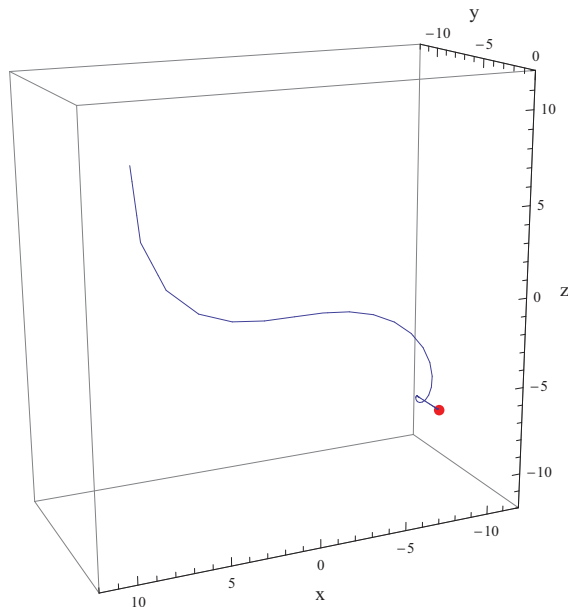


**Figure 11:** One of the off-equatorial stable points depicted in red for  $\mu = 0.1$ ,  $r = 2$ ,  $f = 3$  and  $F_1 = 7$ . Starting from  $(8, -5, 8)$  (depicted) and many other possible initial conditions the centre-of-mass moves towards the stable point.

might cause the centre-of-mass to move away from the equatorial plane. When this happens density differences between the north and south side of the basin occur, meaning one of these sides is warmer. This could be one of the features of El Niño. With only zonal buoyancy fluxes no periodic or chaotic solutions are found in this approximation.

### 5.2.3 Vertical differential buoyancy fluxes

The last situation we will consider is the case with only vertical differential buoyancy fluxes ( $F_3 \neq 0$ ,  $T_2 = F_1 = 0$ ) using the same approach as in the previous sections. This situation with only  $F_3$  corresponds for example with differential heat input from the air above the surface ( $F_3 < 0$ ) or with evaporation ( $F_3 > 0$ ). For the situation in the equatorial plane ( $Y_0 = 0$ ) we now find the equilibrium points to be  $(0, 0, \frac{F_3}{\mu})$  and  $(\pm\sqrt{F_3 - \mu}, 0, 1)$ . These last two points are only real when  $F_3 > \mu$ . To see if they are stable we again use the Jacobian matrix (67).

For  $(0, 0, \frac{F_3}{\mu})$  the eigenvalues are  $\frac{F_3}{\mu} - 1$ ,  $\frac{aF_3}{\mu} - 1$  and  $-\mu$ . We need  $F_3 < \mu$  for the first eigenvalue to be negative. Since  $a < 1$  this way  $F_3 < \mu < \frac{\mu}{a}$ , so the second eigenvalue is also negative. Beside this we know  $-\mu$  is negative, so the only condition needed for stability is  $F_3 < \mu$ . Physically this means the forcing does not force the centre-of-mass up so strong diffusion can not compensate. When this point is stable, there will be no rotation in the basin as  $\mathbf{L} = 0$  according to (43), (44) and (45).

For  $(\pm\sqrt{F_3 - \mu}, 0, 1)$  we find  $-\frac{2}{\mu}(F_3 - \mu)$ ,  $a - 1 \mp b\sqrt{F_3 - \mu}$  and  $-\mu$  as eigenvalues. The first will always be negative, since it is necessary that  $F_3 > \mu$

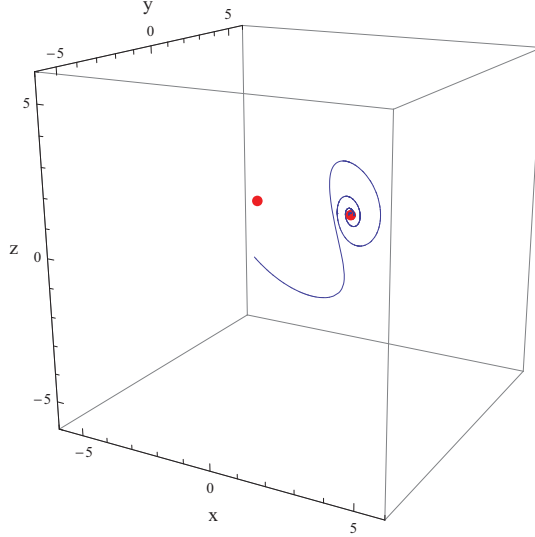


**Figure 12:** Both stable points for  $F_3 > \mu$  depicted in red for  $\mu = 0.8$ ,  $r = 2$ ,  $f = 5$  and  $F_3 = 4$ . Starting from  $(-5, 5, -3)$  (depicted) and many other possible initial conditions the centre-of-mass moves towards one of the stable points.

for these fixed points to exist. Also the last is negative as before. For stability we thus need  $\mp\sqrt{F_3 - \mu} < \frac{1-a}{b}$ . As the right side is always positive ( $a < 1$ ), the plus root (corresponding with a minus sign in the eigenvalue) will always be stable. For the minus root we need  $F_3 < \frac{(a-1)^2 + \mu b^2}{b^2}$  for stability.

When the centre-of-mass is forced upwards the centre-of-mass is more likely to end up at the east side of the basin, corresponding with warmer water in the west. The angular momentum in these cases will be  $\mathbf{L} = (0, \pm\sqrt{F_3 - \mu}, 0)$ , this means that the direction of rotation in the basin depends on the location of the centre-of-mass. Here a clockwise rotation is more likely to occur, as  $(\sqrt{F_3 - \mu}, 0, 1)$  is stable in more cases.

For the equilibrium points outside the equatorial plane ( $aZ_0 - bX_0 = 1$ ) we need  $Y_0^2$  to be positive as before. Now we have:

$$Y_0^2 = \frac{(\mu - aF_3)(b^2(F_3 - \mu) - (a-1)^2)}{(a(a-1))^2 + \mu b^2} \quad (75)$$

This is positive when  $F_3$  is in between  $\frac{\mu}{a}$  and  $\frac{(a-1)^2 + \mu b^2}{b^2}$ , which are both always positive. When this fixed point exists, we use for its stability again the Jacobian matrix (71). The corresponding eigenvalues, as given in Section 5.2.2, are  $Z_0 - 1$ ,  $\frac{2b^2 Y_0^2}{Z_0 - 1}$  and  $-\frac{a(a-1) + \mu b^2}{b^2}$ .

To see if the eigenvalues are negative we have to look at  $X_0$  as  $Z_0 - 1 = -\frac{bY_0^2}{X_0}$ . With only vertical differential buoyancy fluxes  $X_0 = \frac{-\mu b + abF_3}{a(a-1) + \mu b^2}$ . Because  $\mu b^2 > a(1-a)$  is necessary for the last eigenvalue to be negative, we need  $F_3 > \frac{\mu}{a}$  for  $X_0$  to be positive. So it is necessary that  $\frac{\mu}{a} < \frac{(a-1)^2 + \mu b^2}{b^2}$ , as otherwise the points are not real. This corresponds to  $\mu b^2 < a(1-a)$ . This never occurs. So

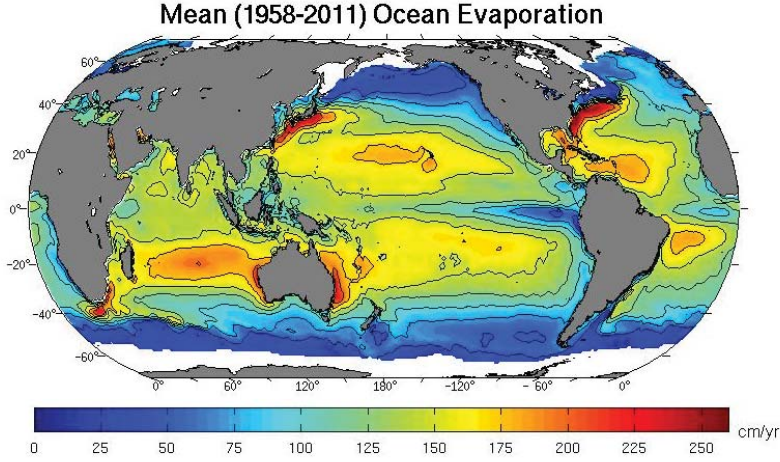


**Figure 13:** The mean ocean evaporation on earth during 1958-2011. On the equator evaporation is lower than at higher latitudes. [13]

these equilibrium points are never stable.

Now we wonder whether the centre-of-mass will always move towards (one of) the equilibrium point(s). When  $F_3 < \mu$  this is the case. To show this, we first translate in such a way that the fixed point is located at the origin. This translation takes  $Z$  to  $Z + \frac{F_3}{\mu}$ . In the same way as in the previous sections we look at the dot product of  $\dot{\mathbf{X}}$  with the outer normal of a sphere centred at the origin. This yields:

$$-x_n^2 \left(1 - \frac{F_3}{\mu}\right) - y_n^2 \left(1 - \frac{aF_3}{\mu}\right) - \mu z_n^2 \quad (76)$$

Since  $F_3 < \mu$  and  $a < 1$ , both  $1 - \frac{F_3}{\mu}$  and  $1 - \frac{aF_3}{\mu}$  are positive and thus (76) is always negative. So for  $F_3 < \mu$  the centre-of-mass will always move towards  $(0, 0, \frac{F_3}{\mu})$ .

When  $F_3 > \mu$  plots indicate that the centre-of-mass always will move towards one of the fixed points (Figure 12), this however is hard to prove. Depending on the initial conditions it will go to  $(\sqrt{F_3 - \mu}, 0, 1)$  or  $(-\sqrt{F_3 - \mu}, 0, 1)$ . In the equatorial plane for positive  $X$  the centre-of-mass will move towards the plus root, whilst for negative  $X$  it moves towards the negative root when this is stable. When the initial location is further away from the equatorial plane, the plus root is reached more often than the minus root.

In the case where only vertical differential buoyancy fluxes are present, there is at least one equilibrium point in the equatorial plane;  $(0, 0, \frac{F_3}{\mu})$ . This point is stable only when  $F_3 < \mu$  and in that case the centre-of-mass will always move towards this fixed point. This happens when for example solar radiation heats the ocean surface ( $F_3 < 0$ ), as is often the case on the equator. In this case there also will be no rotation in the basin, meaning the density increases only with increasing depth.

Two new equilibrium points are found when the vertical forcing becomes strong enough to be no longer compensated by diffusion ( $F_3 < \mu$ ). In that case

the previous fixed point is no longer stable. Of these two points  $(\sqrt{F_3 - \mu}, 0, 1)$  is always stable, whereas it is necessary that  $F_3 < \frac{(a-1)^2 + \mu b^2}{b^2}$  for  $(-\sqrt{F_3 - \mu}, 0, 1)$  to be stable. This situation occurs when for example evaporation is important. In this case also rotation around the  $y$ -axis of order  $\sqrt{F_3 - \mu}$  will occur. In most cases this will be a clockwise rotation in the equatorial plane.

On the equator evaporation is lower than in the surrounding areas as can be seen in Figure 13. Thus we expect, taking only differential buoyancy fluxes into account, there will be one stable equilibrium point somewhere below the geometrical centre. This corresponds to the case where differential heat input by the sun dominates. During an El Niño we do not expect this to change. So only vertical differential buoyancy fluxes do not add much to the dynamics. In combination with other forcing mechanisms this may change. In Section 6 we will discuss the effects of combined forcings, specifically focussing on El Niño.

## 6 El Niño

In the previous sections we have considered various approximations of (4) and (5). In this section we will use both the equations for  $Pr \rightarrow \infty$ , as the initial equations (4) and (5) to investigate what this low order model can say about El Niño. First we will look at the important forcings in the regular situation and compare these with the situation where an El Niño takes place. When this is clear we will see what our model tells us about this. Also we will look at the consequences of seasonal periodicity using our low order model.

### 6.1 Forcings during El Niño

In the normal situation, the two main forcings of the circulation in the Pacific Ocean are the trade winds and the heating of water by the sun. The sun heats the water at the surface ( $F_3 < 0$ ) and thus causes a temperature difference between surface and bottom ( $Z < 0$ ). The trade winds blow westward ( $T_2 < 0$ ) and this way force the warm surface water towards the west side of the basin ( $X > 0$ ). Here the water will move downwards due to gravity, while at the east side upwelling will take place ( $L_2 < 0$ ). These processes are shown in Figure 14.

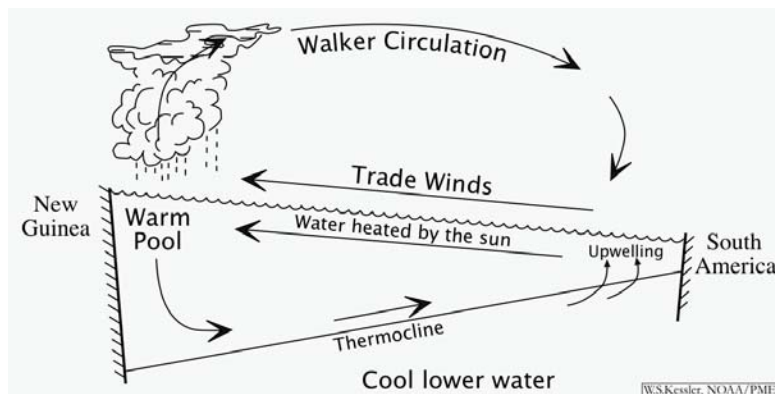
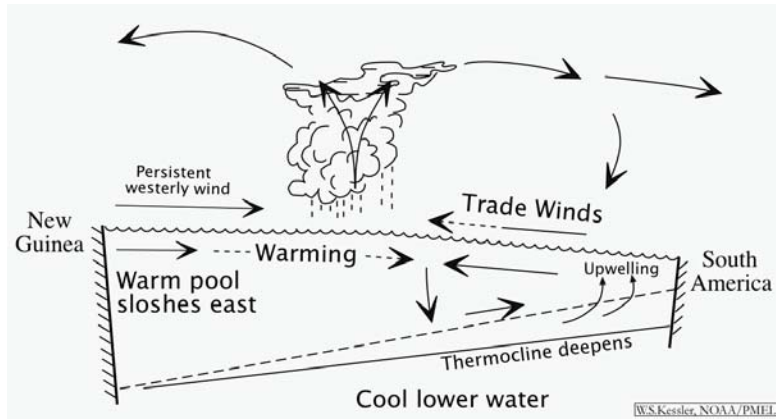


Figure 14: The dynamics governing the Pacific Ocean in the normal situation. [14]



**Figure 15:** The dynamics governing the Pacific Ocean during an El Niño. [14]

Then, what happens when an El Niño takes place? In that case the trade winds are weaker, which weakens the temperature difference between east and west ( $X$  getting smaller). This is shown in Figure 15. The consequence of this weaker temperature difference is that the warm surface water descends more towards the centre of the ocean (reduced  $L_2$ ). The circulation of the ocean changes. The sea surface temperature over the whole basin is also higher than usual ( $Z$  being more negative).

The differential heat input by the sun remains the same during an El Niño. In Section 6.2 we will look at a normal and El Niño situation where the only forcings are the trades ( $T_2$ ) and differential heat input by the sun ( $F_3$ ). This means the situation is symmetric in the equatorial plane. We will numerically solve the system using both the approximation  $Pr \rightarrow \infty$  (Section 5), as the initial equations (4) and (5) (Section 2).

## 6.2 Dynamics of El Niño

As it is hard to estimate realistic values for the parameters, like  $\mu$  and  $T_2$ , it is important to look at the differences between certain situations. We use *Dynamics Solver* to solve the equations numerically for different values of  $T_2$ . All other parameters remain constant through all these computations. Some of the results are shown in Figure 16. Note that using both the initial equations, as the approximation  $Pr \rightarrow \infty$  the same equilibrium points are found, but the paths towards them differ.

In the normal situation the trades are quite strong. In that case our equilibrium point is located in the equatorial plane with  $X > 0$  and  $Z = 0$  (Figure 16).  $Z$  being zero means the density difference between the east and west side is more important than the density difference between surface and bottom. In this situation the angular momentum  $L_2$  turns out to be quite strong, around -8 using the initial equations. This indicates there is a lot of rotation in the equatorial plane due to the strong wind forcing.

In the situation of an El Niño the trades are weaker. As a consequence the equilibrium point lies a lot deeper and also the  $X$  part is larger. Here the density

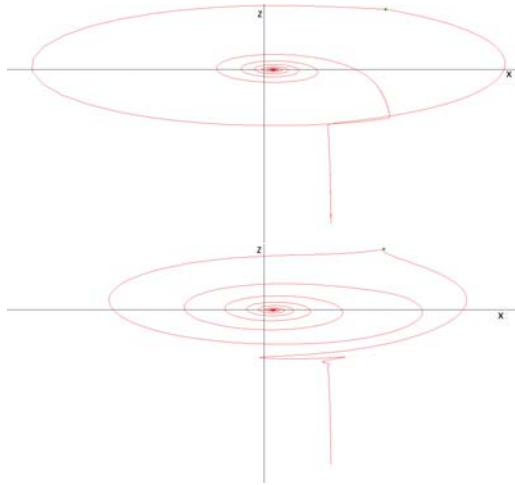


**Figure 16:** The paths of the centre-of-mass projected on the equatorial plane starting from  $(7, 3, 14)$  (green dots) for different values of  $T_2$ . The upper figure shows the trajectory using  $Pr \rightarrow \infty$  and the lower using the initial equations. The used parameters are  $\mu = 0.1$ ,  $r = 0.4$ ,  $f = 2$  and  $F_3 = -4$ . The circle-like paths are found when  $T_2 = -8$ , the others when  $T_2 = -4$ .

difference between surface and bottom is more important than the difference in the zonal direction. A consequence is the weakening of the rotation in the basin, around  $-0.3$  compared with  $-8$  in the normal situation. In the normal situation the angular momentum keeps pace with the strength of the trades, which is not the case any more during an El Niño.

When looking at wind strengths in between  $-4$  and  $-8$  we see there is a sudden jump in the location of the equilibrium point between  $5.4$  and  $5.5$  (with the numerical values given at Figure 16). This jump might indicate the transition from the normal state to an El Niño state. As the strength of the trade winds gets below a critical value, the vertical density differences get more important than the zonal differences. This indicates that the sea surface temperature will be more equal over all longitudes, weakening the trade winds even more and so sustaining this situation.

Thus by only changing the strength of the trade winds ( $T_2$ ) a transition from the normal to the El Niño situation is found. This does mean we need the atmosphere as input. The ocean alone can not explain the occurrence of El Niño when we take only the trades ( $T_2$ ) and solar heating ( $F_3$ ) into account. By looking at more parameters periodic and even chaotic solutions might be found. In Section 6.3 we will look at seasonal variations keeping El Niño in mind.

### 6.3 Seasonal variations

In all cases we have considered so far we have looked at the forcings which are symmetric in the equatorial plane ( $F_1$ ,  $F_3$  and  $T_2$ ). But most of the time the forcings in the area near and at the equator are not symmetric. For example a seasonal variability in heat input by solar radiation takes place, altering the latitude at which most solar radiation is received. As a consequence the winds

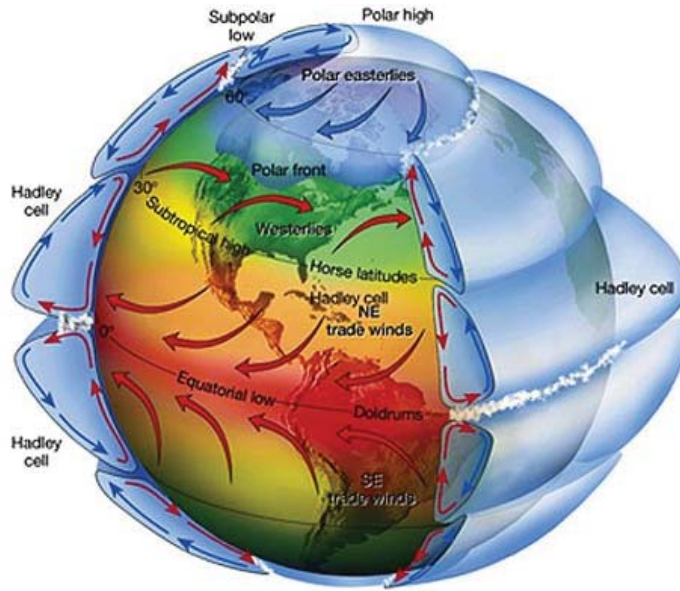


**Figure 17:** The atmospheric circulation of the earth, including the Hadley Cell, the Intertropical Convergence Zone and the trade winds. [15]

are not completely westward. These seasonal variations change the dynamics of the system.

Due to the earth's obliquity<sup>2</sup>, the region of highest incoming solar radiation oscillates during the year. In Southern Hemisphere summer this region is located at about 30 degrees south ( $F_2 > 0$ ) and vice versa ( $F_2 < 0$ ) when it is summer in the Northern Hemisphere. These seasonal changes of the incoming solar radiation affect the dynamics of the atmosphere. Where most solar radiation is received the air heats most and thus rises. High in the atmosphere this air is transported towards the poles. At latitudes around  $\pm 30$  degrees it sinks and moves back towards the equator near at the surface. This circulation is known as the Hadley Circulation (Figure 17) [2].

Due to the Coriolis force the surface winds blowing towards the equator are deflected westwards and form the trade winds. The region where the trade winds come together is called the Intertropical Convergence Zone [2]. As the location of the Hadley Cells changes with the seasons, so does the location of the Intertropical Convergence Zone (ITCZ, Figure 18). As a consequence the wind at the equator is south-west ( $T_2 < 0, T_1 > 0$ ) during the Southern Hemisphere summer and north-west ( $T_2 < 0, T_1 < 0$ ) during the Northern Hemisphere summer. Another effect is the occurrence of wind torque. Since in Southern Hemisphere summer the wind at the north side is more to the south and at the south side more to the west ( $T_3 < 0$ ), a horizontal rotation in the ocean is induced ( $L_3 < 0$ ).

In this section we will investigate the consequences of certain seasonal forc-

<sup>2</sup>Obliquity is the angle between the rotational axis of the earth and the orbital axis between the earth and the sun (approximately  $23^\circ$ ).



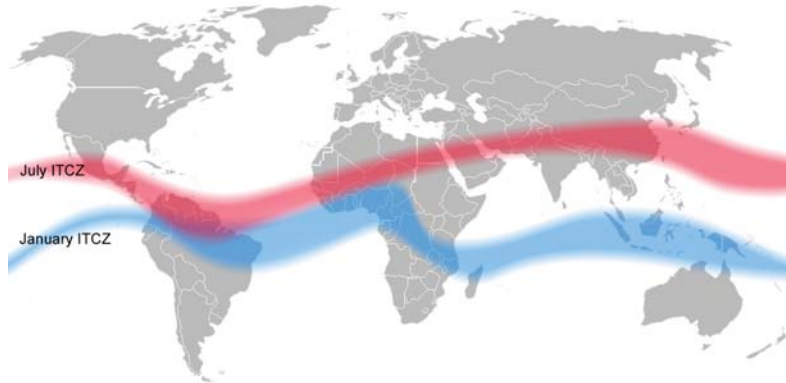


**Figure 18:** The average location of the Intertropical Convergence Zone during January and July. [16]

ings. For this we will numerically integrate (4) and (5) using *Dynamics Solver*. The different forcing strengths used, are found by trial and error and so do not give a complete overview of the occurring dynamics. In all cases we take  $Pr = 5$ ,  $f = 2$ ,  $r = 0.4$  and  $\mu = 0.1$ .

First we look at what happens when there is differential heating in the meridional direction ( $F_2$ ). In this case for strong forcing a periodic trajectory is found (Figure 19). This closed path around the  $y$ -axis has positive  $y$  for positive  $F_2$ , and negative  $y$  for negative  $F_2$ . When it is summer in the Northern Hemisphere the centre-of-mass will be located at the Southern Hemisphere and vice-versa. This is expected as the warmer less denser water is located at the summer hemisphere. El Niño is strongest in December and January, when it is summer at the Southern hemisphere. This is the moment  $F_2$  is largest, which corresponds to the largest ‘radius’ of the trajectory.

Together with the change of differential heating in the meridional direction, also the wind in these direction changes ( $T_1$ ). Positive  $T_1$  correspond to positive  $F_2$  according to the right-hand rule and similarly negative  $T_1$  correspond to negative  $F_2$ . Now when the meridional winds ( $T_1$ ) become strong no periodic solutions are found, while for weaker winds there are. This is only the case when also meridional differential heating is present. Only wind in the meridional directions does not yield periodic solutions.

Also wind torque ( $T_3$ ) is likely to contribute to the seasonal variability. When it is summer in the Southern Hemisphere, the wind torque will be negative (counterclockwise), as the Intertropical Convergence Zone lies south of the equator. Just like the meridional winds, only wind torque does not yield periodic behaviour. Combined with meridional differential heating ( $F_2$ ) it does. Then however it should not be too large. In the presence of  $T_3$  periodic solutions for larger  $T_1$  are found than previously.

Seasonal variability causes periodic trajectories of the centre-of-mass at one side of the equator. These trajectories change together with the seasons and thus might provide some information about the seasonal dependence of El Niño. When the dynamics of the atmosphere is focussed at one side of the equator, the found periodic trajectories could describe the El Niño-La Niña oscillation.



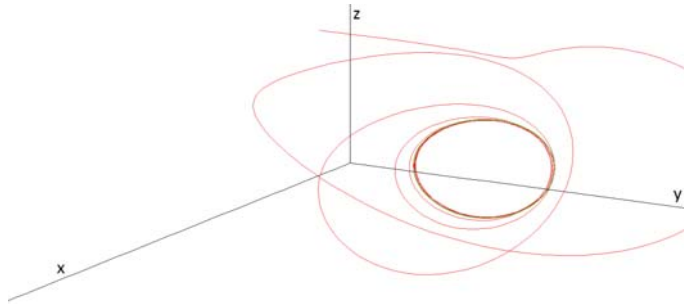


**Figure 19:** The trajectory of the centre-of-mass starting from  $(7, 3, 14)$  when  $T_2 = -8$ ,  $F_3 = -4$  and  $F_2 = 8$ . In green the final periodic trajectory is shown.

The location of the ITCZ in January and July (Figure 18) does not indicate this is the case at the Pacific Ocean, so other explanations are needed.

## 7 Discussion and conclusion

We have used a low order model to look at the ocean near and at the equator. In various approximations we have computed trajectories and (stable) equilibrium points when possible, focussing on the dynamics of the El Niño-La Niña oscillation.

In Section 3 and 4 we have investigated the inertial dynamics of the system without diffusion and viscosity. The pendulum motion in the equatorial plane indicates the warmer less denser water oscillates between the east and west side of the basin when this motion is not damped. Forcing mechanisms, like differential heating in the zonal direction ( $F_1$ ), alter this path.

In Section 5 we approximated the equations by assuming that the mixing of momentum occurs faster than the mixing of temperature and salt. This way we found equilibrium points for cases with only one equatorial symmetric forcing at a time. Most of these fixed points are located in the equatorial plane, but for certain negative differential buoyancy fluxes in the zonal direction ( $F_1$ ) stable points outside the equatorial plane are found. These stable points show what the effect is of each forcing separately. It however does not provide much information on what happens when you combine them.

To focus on El Niño we looked at numerical solutions of both the initial equations (4), (5), as the approximation  $Pr \rightarrow \infty$  (46), (47), (48) in Section 6. A difficulty is that the values of the parameters are not well known. With more knowledge of the parameters, more could be concluded from this numerical results. Now we have to compare different situations to see what the effects of different forcing mechanisms are.

Still the numerical results using this low order model can explain already some features of El Niño. Changing of only the strength of the trade winds results in a downward jump of the centre-of-mass. This jump means that the vertical density differences become more important than the zonal differences, indicating a very small temperature difference between the east and west side of the Pacific Ocean. This probably corresponds to an El Niño. The periodic

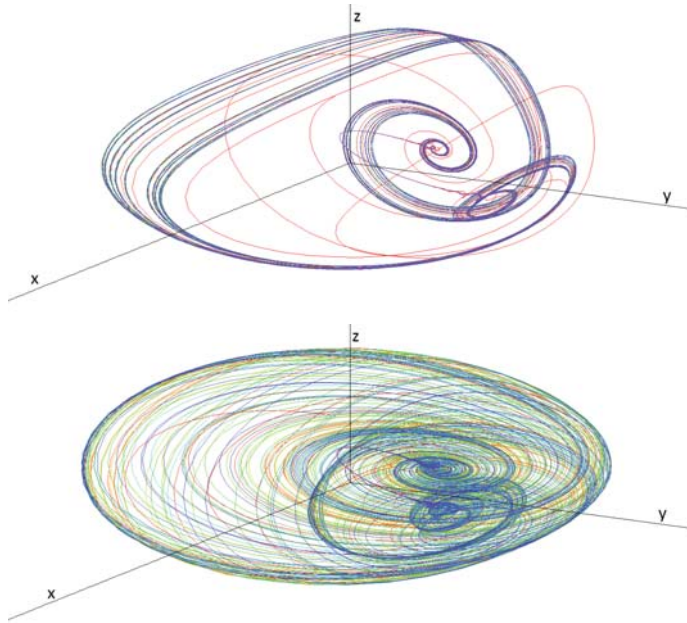


**Figure 20:** The trajectories of the centre-of-mass starting from  $(7, 3, 14)$ . The upper figure shows the trajectory using  $Pr \rightarrow \infty$  and the lower using the initial equations (with  $Pr = 5$ ). The used parameters are  $\mu = 0.1$ ,  $r = 0.4$ ,  $f = 2$  and  $F_2 = 15$ ,  $F_3 = 5$ ,  $T_1 = 30$  and  $T_3 = -10$ .

solutions found do not explain El Niño, except when the atmospheric dynamics are focussed on one hemisphere. They could explain the seasonal dependence of the strength of El Niño, but not its full behaviour.

Using this low order ocean-only model, features of El Niño are found. But so far it has not been able to explain El Niño without taking into account the changing forcings of the atmosphere. It might be interesting to make some of the atmospheric forcings periodic in our model. This way it would be possible to add seasonal variability to the equations.

Another interesting extension of our model would be to add a simple atmospheric model. As the trade winds ( $T_2$ ) are very important for the equatorial dynamics, a first simple extension is making the zonal winds dependent on the location of the centre-of-mass, that is  $T_2 = T_2(X)$ . It would be interesting to see if with such a simple extension of our model periodic solutions in the equatorial plane can be found. To further investigate this option Vallis (1988) [17] could be consulted. Here simple ocean-atmosphere models are used to look at El Niño.

Beside the stable equilibrium points and periodic solutions, also chaotic solutions are found using both the approximation  $Pr \rightarrow \infty$  and the initial equations. In Figure 20 situations in which chaos occurs are depicted for both  $Pr \rightarrow \infty$  and the initial equations. The occurring chaos is bounded to a certain area, which differs between the used equations.

In more situations than the one shown in Figure 20 chaos is found. It is not necessary for the vertical buoyancy fluxes ( $F_3$ ) to be positive, but when they

are not, the other forcing mechanisms have to be very strong. Positive  $F_3$  might however occur when a lot of evaporation takes place. Also westward winds ( $T_2 < 0$ ) reduce the number of situations where chaos is found. The same holds for zonal buoyancy fluxes ( $F_1$ ) being negative, for example differential heat input at the east. In none of the tried situations chaotic trajectories corresponding to El Niño are found.

In all our computations we have used a non-conventional term for the Coriolis force. This alters the direction in which the initial oscillation takes place and causes most of the dynamics to happen in the equatorial plane. This is also the direction in which most of the dynamics of the El Niño-La Niña oscillation takes place. Seasonal variations cause a breaking of this symmetry, resulting in off-equatorial stable points and periodic trajectories. The used Coriolis parameter is important in the occurrence of these trajectories as it makes sure that most of the dynamics still are quite parallel to the equatorial plane.

Our low order ocean-only model quite well explains what happens to the ocean under certain atmospheric forcings. It also shows nicely some of the features of El Niño, but the El Niño-La Niña oscillation has not been found. For this the atmosphere has presumably to be included. It is interesting to investigate what the consequences for the dynamics are if a simple atmospheric model is added, starting with the zonal winds. Maybe such a model can explain the El Niño-La Niña oscillation.

## A Reducing to three equations

To reduce the equations of Section 3 we start using the second invariant (13) (stratification) to remove the first variable. To do so, we write  $X$ ,  $Y$  and  $Z$  in spherical coordinates  $c_2 > 0$ ,  $\theta \in [0, \pi]$  and  $\phi \in [0, 2\pi[$ , where  $c_2$  is fixed:

$$X = c_2 \sin \theta \cos \phi \quad Y = c_2 \cos \theta \quad Z = c_2 \sin \theta \sin \phi \quad (77)$$

We calculate the derivatives of these expressions and insert these together with (77) in the differential equations for  $\mathbf{X}$  (9), (10) and (11). This way we find after some calculations the derivatives of  $\theta$  and  $\phi$ :

$$\dot{\theta} = L_1 \sin \phi - L_3 \cos \phi \quad (78)$$

$$(\dot{\phi} + L_2) \sin \theta = \cos \theta (L_1 \cos \phi + L_3 \sin \phi) \quad (79)$$

Now we have reduced the set of six equations to a set of five. To reduce this set further, we change to cylindrical coordinates  $r$  and  $\alpha \in [0, 2\pi[$  for  $L_1$  and  $L_3$ :

$$L_1 = r \cos \alpha \quad L_3 = r \sin \alpha \quad (80)$$

The corresponding differential equations are found using the differential equations for  $L_1$  and  $L_3$ , (6) and (8), and the derivatives of (80). For  $r$  and  $\alpha$  we this way find:

$$\dot{r} = -c_2 \cos \theta \cos \alpha \quad (81)$$

$$(\dot{\alpha} - 1)r = c_2 \cos \theta \sin \alpha \quad (82)$$

In this new coordinates we can reduce the set of equations further by solving the first invariant (12) (energy) for  $L_2$ , resulting in:

$$L_2 = \pm \sqrt{2c_1 - 2c_2 \sin \theta \sin \phi - r^2} \quad (83)$$

Now we insert all the above in the last invariant (14) (momentum) and solve the resulting equation for  $\alpha$  to find:

$$\alpha = \phi - \arccos\left(\frac{c_3 - c_2 \cos \theta (1 \pm \sqrt{2c_1 - 2c_2 \sin \theta \sin \phi - r^2})}{c_2 r \sin \theta}\right) \quad (84)$$

Note this equation is only valid when the term in the arccosine is in between plus and minus one. Using the above equations for  $L_2$  and  $\alpha$  we find a set of three differential equations in  $r$ ,  $\theta$  and  $\phi$ :

$$\dot{r} = -c_2 \cos \theta \cos\left(\phi - \arccos\left(\frac{c_3 - c_2 \cos \theta (1 \pm \sqrt{2c_1 - 2c_2 \sin \theta \sin \phi - r^2})}{c_2 r \sin \theta}\right)\right) \quad (85)$$

$$\dot{\theta} = \frac{\sqrt{c_2^2 r^2 \sin^2 \theta - (c_3 - c_2 \cos \theta (1 \pm \sqrt{2c_1 - 2c_2 \sin \theta \sin \phi - r^2}))^2}}{c_2 \sin \theta} \quad (86)$$

$$\dot{\phi} = \frac{\mp c_2 \sqrt{2c_1 - 2c_2 \sin \theta \sin \phi - r^2} + \cos \theta (c_3 - c_2 \cos \theta)}{c_2 \sin^2 \theta} \quad (87)$$

## References

- [1] Tropical Ocean Atmosphere Project: 2014, *El Niño Theme Page*, National Oceanic and Atmospheric Administration, consulted on 3 June 2014.
- [2] Cushman-Roisin, B., Beckers, J.: 2011, *Introduction to Geophysical Fluid Dynamics*, Elsevier.
- [3] Taylor, J.R.: 2005, *Classical Mechanics*, University Science Books.
- [4] Maas, L.R.M.: 2004, 'Theory of Basin Scale Dynamics of a Stratified Rotating Fluid', *Surveys in Geophysics* **25**, 249-279.
- [5] Maas, L.R.M.: 1994, 'A Simple Model for the Three-dimensional, Thermally and Wind-driven Ocean Circulation', *Tellus* **46A**, 671-680.
- [6] Haren, van, H.: 2005, 'Sharp Near-equatorial Transitions in Inertial Motions and Deep-ocean Step-formation', *Geophysical Research Letters* **32**, L01605.
- [7] Pedlosky, J.: 1987, *Geophysical Fluid Dynamics*, Springer, New York.
- [8] Ertel, H.: 1942, 'Ein Neuer Hydrodynamischer Wirbelsatz', *Meteorologische Zeitschrift* **59**, 277-281.
- [9] Stewart, R.H.: 2005, 'Vorticity in the Ocean', *Introduction to Physical Oceanography*, Texas A&M University.
- [10] Olver, F.W.J., Lozier, D.W., Boisvert, R.F. and Clark, C.W.: 2010, *NIST Handbook of Mathematical Functions*, Cambridge University Press, New York.
- [11] Lorenz, E.N.: 1963, 'Deterministic Nonperiodic Flow', *Journal of the Atmospheric Sciences* **20**, 130-141.
- [12] Schrier, van der, G., Maas, L.R.M.: 2000, 'The Diffusionless Lorenz Equations: Shil'nikov Bifurcations and Reduction to an Explicit Map', *Physica D* **141**, 19-36.
- [13] Yu, L., Weller, R.A. and Jin, X.: 'Ocean Evaporation Products', *Objectively Analyzed air-sea Fluxes (OAFlex) for the Global Oceans*, Woods Hole Oceanographic Institution, consulted on 11 June 2014.
- [14] Kessler, W.S.: 'Frequently Asked Questions about El Niño', *Home Page of William S. Kessler*, National Oceanic and Atmospheric Administration and School of Oceanography, University of Washington, consulted on 7 June 2014.
- [15] NASA: 2005, 'Atmospheric Circulation; Weather Systems', *The Water Planet - Meteorological, Oceanographic and Hydrologic Applications of Remote Sensing*, consulted on 11 June 2014.
- [16] Halldin, M: 2006, 'Intertropical Convergence Zone', *Wikipedia*, consulted on 11 June 2014.
- [17] Vallis, G.K.: 1988, 'Conceptual Models of El Niño and the Southern Oscillation', *Journal of Geophysical Research* **93**, 13,979-13,991.